mechanical engineering research

Final Report

Work Function Determination of Promising Electrode Materials for Thermionic Converters

To: NASA Lewis Research Center
NASA Grant ~~NGS~~ NSG-07019

by
Dean Jacobson

center for research

college of engineering & applied sciences

engineering • agriculture • technology • construction

arizona state university
tempe, arizona 85281

I. Introduction

Work performed on NASA Grant NSG-07019 was primarily for the evaluation of selected electrode materials for thermionic energy converters. The original objective was to characterize selected nickel based superalloys up to temperatures of 1400°K. It was found that an early selection, Inconel 800 produced a high vapor pressure which interfered with the vacuum emission measurements. The program then shifted to two other areas in conjunction with Dr. Ed Sotrms at Los Alamos Scientific Laboratories. The first area was to obtain emission from the superalloys in a cesiated atmosphere. The cesium plasma helps to suppress the vaporization interference. The second area involved characterization of the Lanthanum-Boron series as thermionic emitters. These final two areas resulted in three Journal publications which are attached to this report.

II. Vacuum Emission Experiments

1) Vacuum Emission Vehicle

A vacuum emission vehicle was developed especially for measurements taken during this program. The vacuum system (Fig. 1) consists of sorption roughing pumps, titanium sublimation intermediate pumping, and 140 liter/sec Noble gas vac-ion pumping. Samples are heated by electron bombardment from a high temperature counter wound tungsten filament. Sample temperatures are measured with micro-optical pyrometer viewing a 10 to 1 dept to diamter hohlraum. The electron collector consists of a planar one-half-inch-diameter radiation cooled molybdenum electrode as shown in Fig. 2 and 3. The collector is guard ringed by a large molybdenum ring with a 10-mil spacing between collector and guard ring. The vacuum system is completely bakeable and can maintain pressures of 10^{-10}

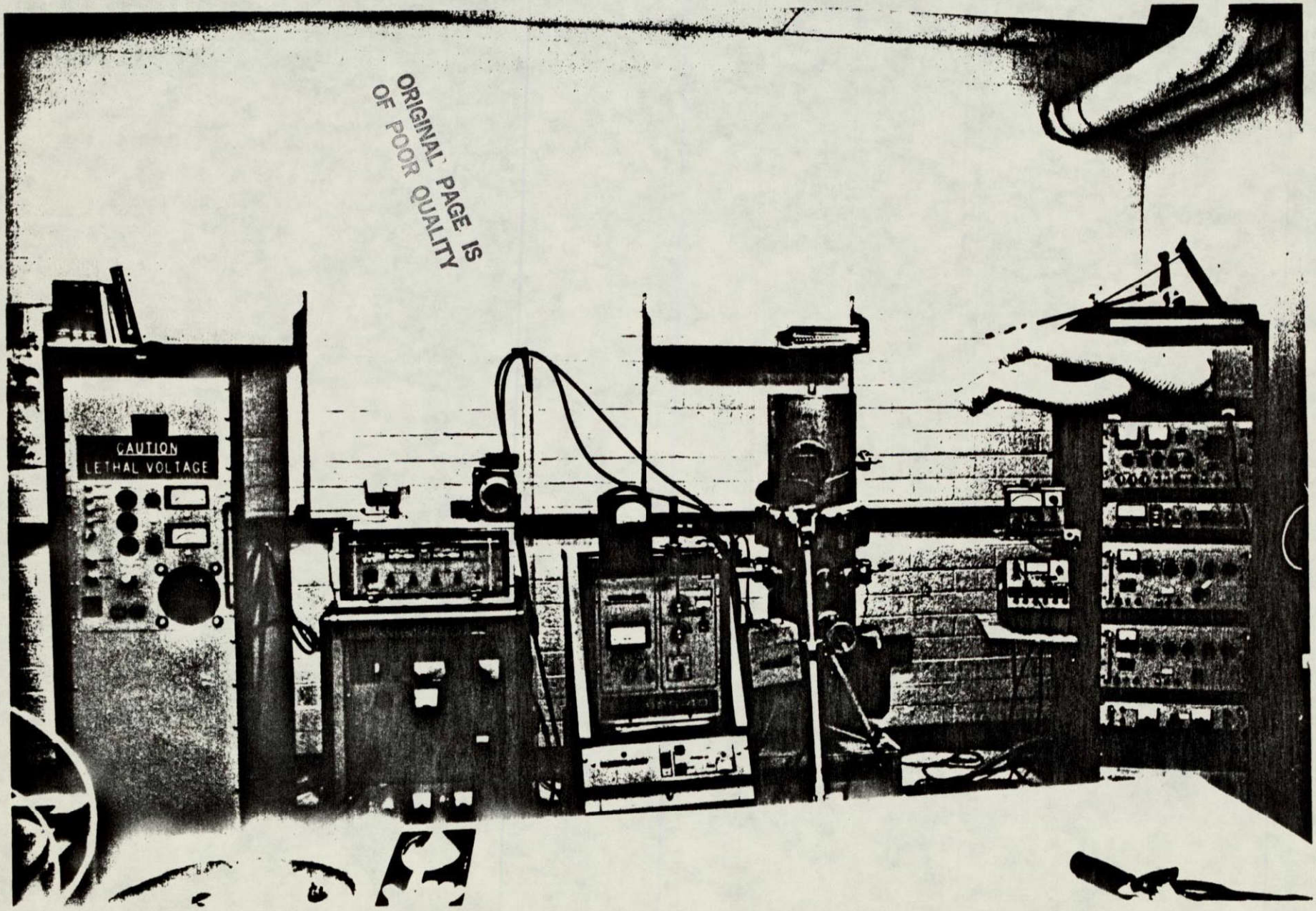

Figure 1

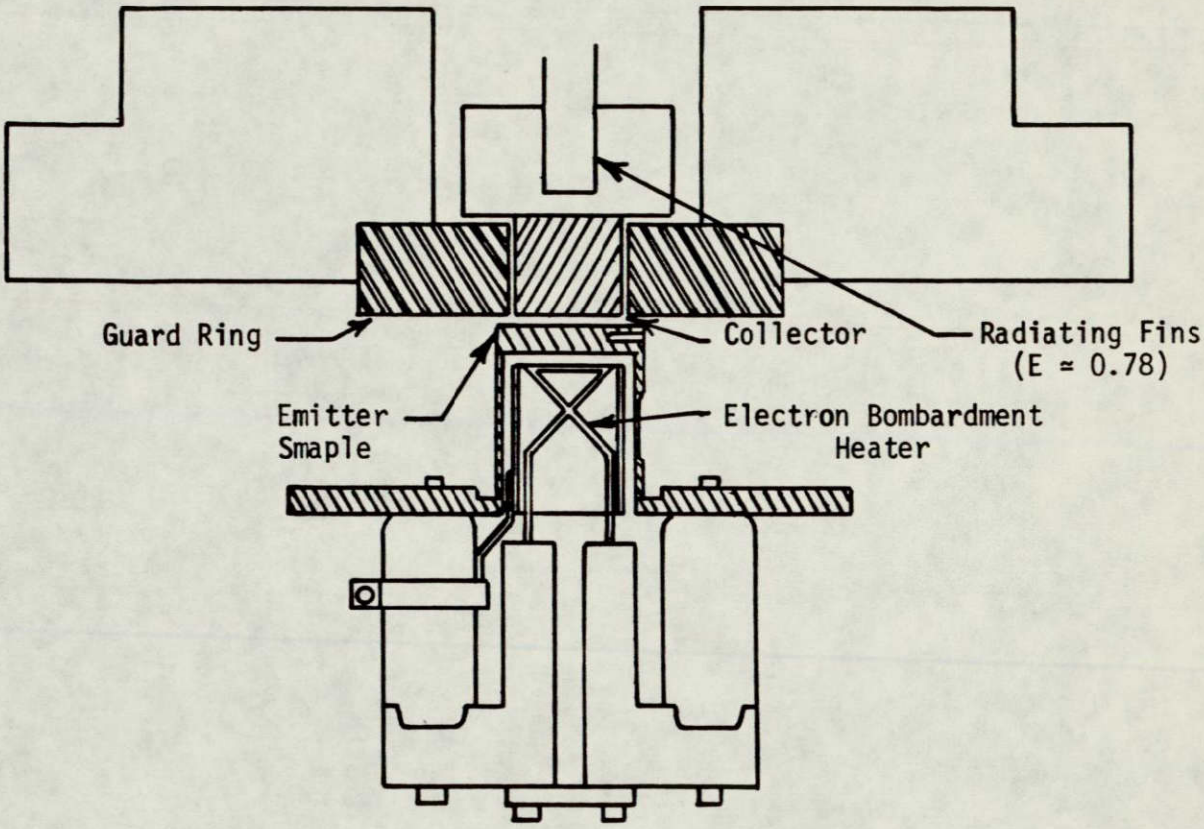

Figure 2 Schematic of Vacuum Emission Test Vehicle

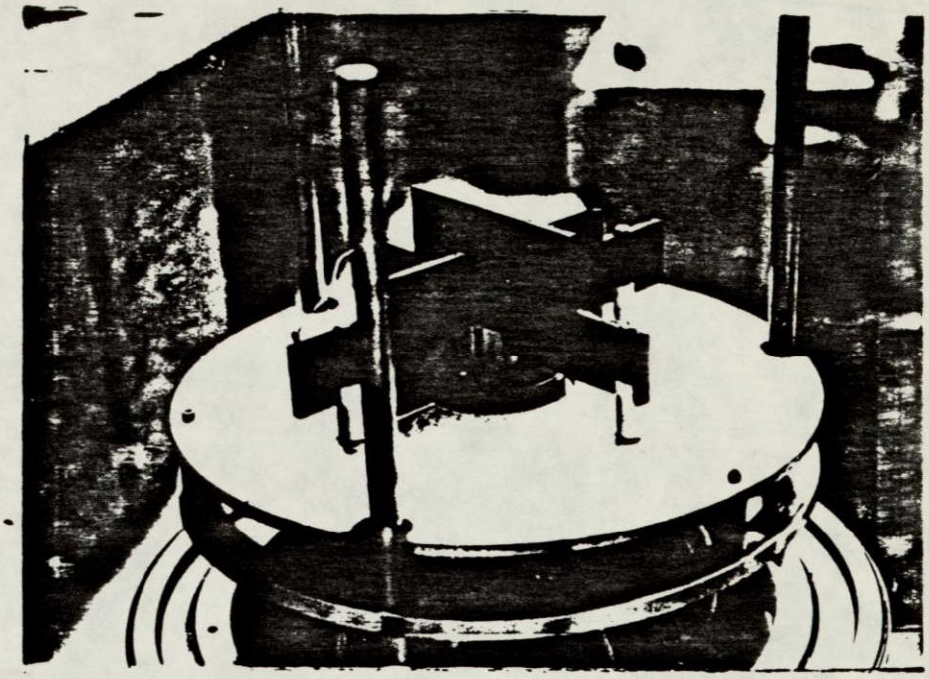

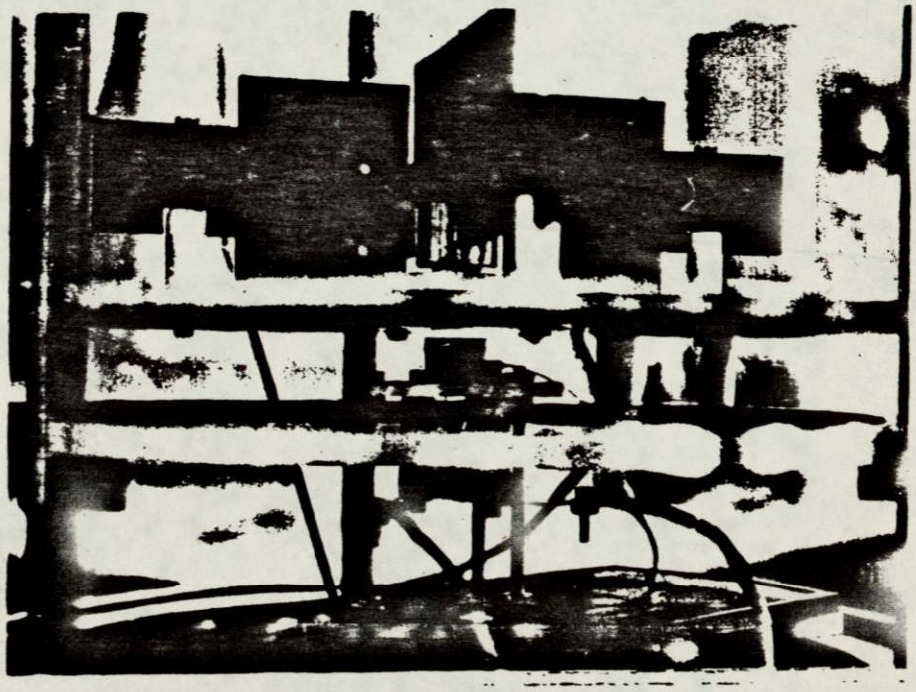

Fig. 3 Vacuum Emission Test Set Up

torr. In the electrical measurement high precision Fluke digital power supplies are connected to the collector and the guard ring. These are then balanced through a null meter.

Experimentally, a potential is set between the emitter and the collector, and current leakage is nulled between collector and guard ring by the second fluke supply connected to the guard ring. The current is then measured with a Keithly micro-microammeter.

2) Thermionic Emission Microscope

The second device, a thermionic emission microscope, contains a Faraday cage for the measurement of the electron emission from individual grains, and a phosphor screen for displaying the fine grain structure for visual observation and subsequent emission micrograph documentation.

Fig. 4 is an assembly drawing of the emission microscope indicating the location of the basic components which are: the emitter sample and heater, the X, Y, and Z traverse mechanism, lenses, screen, Faraday cage, and vacuum system. A guarded Faraday cage was incorporated into the microscope for the purpose of measuring the effective work function of individual grains on the cathode sample. The guard prevents current leakage across insulators in the measuring circuit, since the current measurements to be taken can be below 10^{-11} amp. A Keithley 610R electrometer with a noise level of 4×10^{-14} amp was used to measure the current collected by the Faraday cage. The noise level of the entire current measuring circuit of the microscope is approximately 5×10^{-13} amp. The microscope was adjusted to operate at approximately X80 magnification to accommodate the relatively large grains of the samples investigated. The microscope was operated at a vacuum level of 1×10^{-8}

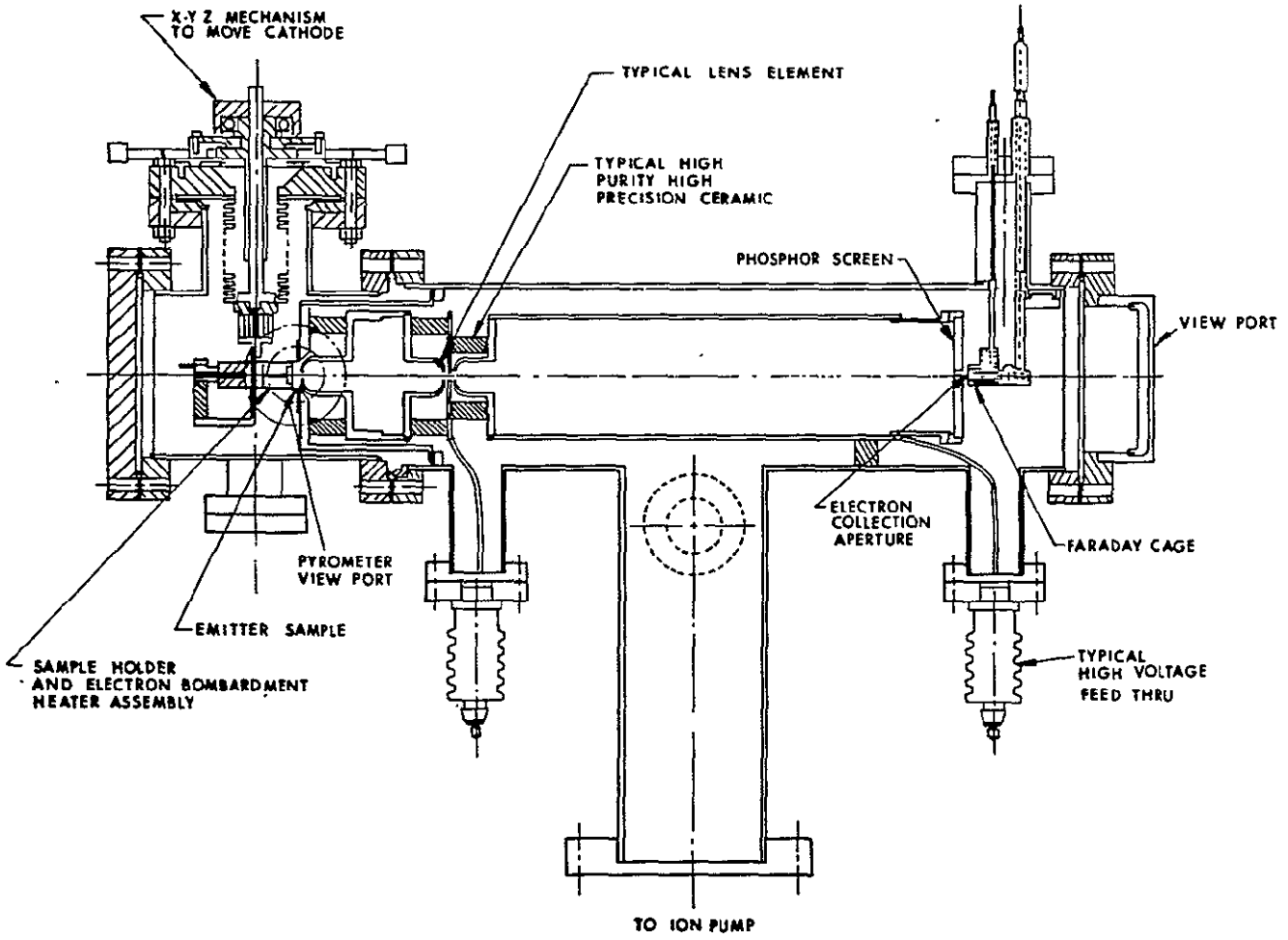

Fig. 4—Thermionic emission microscope assembly and components.

Figure 4

torr at emitter temperatures as high as 2200 K.

The Faraday cage current can be related to the sample electron current density by the following equation:

$$J_0 = \frac{I \cdot M^2}{A_c}$$

where I is the current from the sample as measured in the Faraday cage, M is the magnification at the current collecting plane, A_c is the area of the hole in the center of the screen at the collecting plane, and J_0 is the emitter current density.

The effective work function ϕ is calculated from the Richardson-Dushman equation,

$J_0 = AT^2 \exp [-\phi/kT]$

J_0 is the emitter current density as measured in the vacuum emission vehicle, or with the microscope. T is the emitter temperature. The parameter A has the value 120 amp per sq cm k^2 and in this case ϕ is called the effective work function. k is the Boltzmann constant.

3) Mass Spectrometer

The experimental facilities available at Los Alamos, in addition to the normal facilities expected in a modern well equipped chemical laboratory, are the capability for the preparation of pure materials having the proper compositions and characterization of these materials before and after using chemical and nutronic division analysis by x-ray and nutron diffraction, by scanning electron microscope, and by metallographic examination. A unique mass spectrometer is located at LASL which permits the measurements of vapor pressure and diffusion rates over a very wide range of temperatures.

4) Photon Counting Pyrometer

A photon counting pyrometer has been designed and built which will permit black body temperatures to be determined with a precision of ±0.2K. The basic concept and design were originated by Dr. Edmund Storms at the Los Damos Scientific Laboratory. Several parts were generously supplied by Dr. Storms. Other equipment was obtained from laboratories in the Engineering Department at A.S.U.

In the measurement of quantized radiation fields such as light, most information is obtained by counting individual events corresponding to the individual photons. The counter can be compared to a D.E. analog technique for making light measurements where many photon events are integrated over time, with the result that the photon counting method in a high performance system has at least three major advantages:

a) optimum signal to noise ratio for quantum-limited signals

b) excellent long-term stability

c) wide linear dynamic range

Precision is improved by more than an order of magnitude and repeatability is greatly enhanced when comparing the photon counter to optical pyrometry.

An available Leeds and Northrup pyrometer was modified as shown in Fig. 5. Light from a black body source passes through a narrow band interference filter and is focused onto the metal mirror through the objective lens system. The hohlrom image, where the temperature is to be measured, is focused over the 0.010 cm hole in the mirror. This is done while viewing the image and mirror through the image lens system. The light passing through the mirror hole is attenuated by a choice of neutral density filters, before continuing to the photomultiplier tube. Pulses from the photomultiplier tube are amplified, clipped, and reasmplified by a P.A. R. 1121 Amplifier-

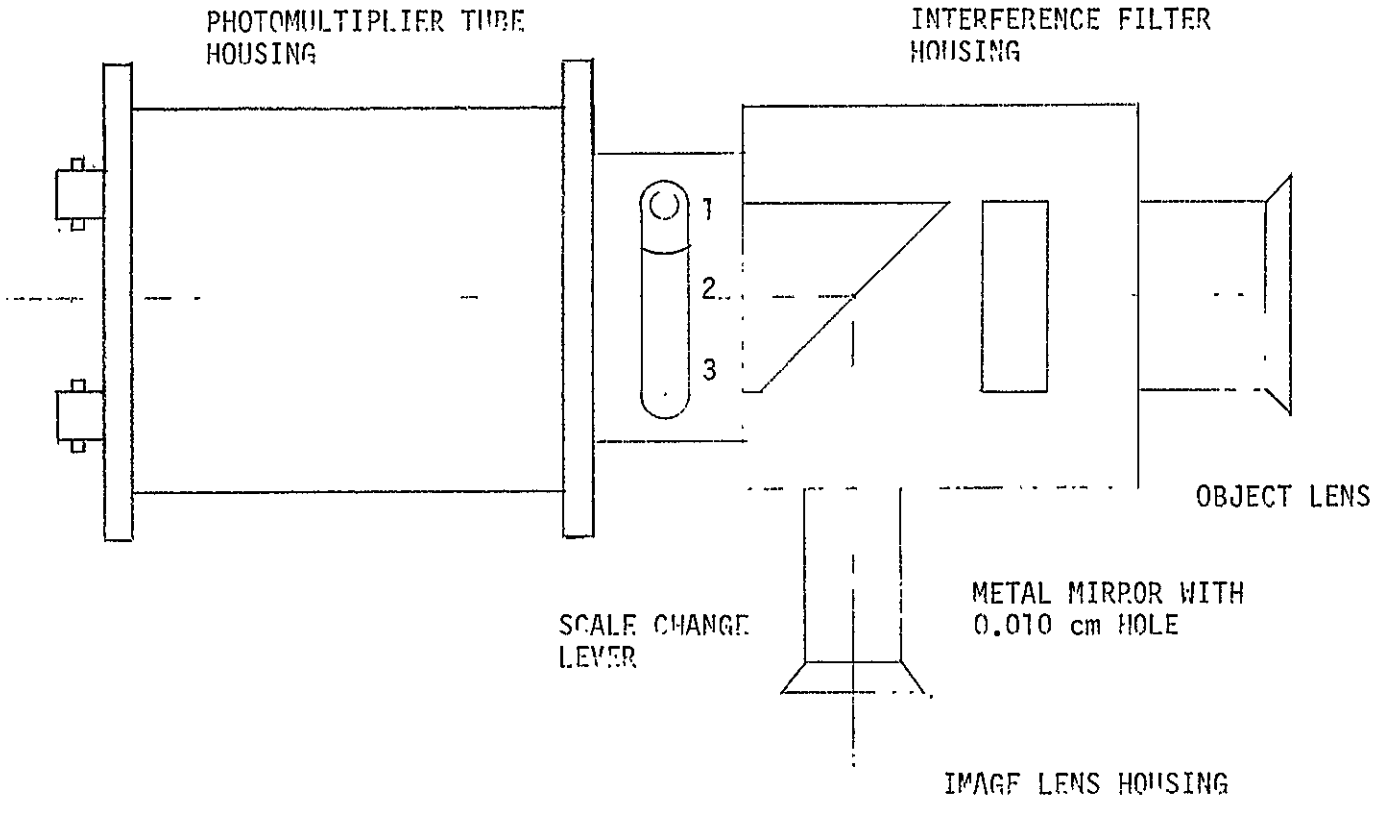

FIGURE 5 TOP VIEW OF PHOTON COUNTING PYROMETER.

System. They are then fed to a Hewlett-Packard 5308A counter. The overall schematic is shown in Fig. 6.

Calibration of the pyrometer requires knowledge of the count rate (R_g) at a known temperature (T_g), the wavelength of the transmission maximum in the interference filer $(\lambda_o)_1$ and Planck's second radiation constant (C_2). L.A.S.L. has offered to let us use their gold furnance for calibration. Planck's law related the count rate, R_c, and the unknown temperature, T_m, through the equation

$$T_m = 1/[(\ln R_g - \ln R_c)\ \lambda_o/C_2 - 1/T_g]$$

where $C_2 = 0.014388\ _{mk}$

$$1/T_g = 7.4762 \times 10^{-4} k^{-1}$$

The measurements are based upon extropolation of the thermodynamic temperature scale above the gold point and the absolute accuracy is thus, in principle, as good as can be obtained. The interference filter has a finite bandwidth, and with the limits of accuracy in the electronics system and elsewhere, the precision is calculated to be better than $\pm$0.2K at 2000K.

5) Emission Measurment Procedures.

The superalloy electrodes were electron-beam machined as single pieces. Each of the samples was fine-polished with Linde alumina A, B, and C, then cleaned chemically in Oakite and ultrasonically in alcohol and distilled water.

Electron emission measurements were taken at a number of emitter temperatures for each sample. At each temperature, the emission was measured as a function of the applied voltage. With this data, the zero field or saturated emission from the metals was determined by generating Schottky plots according to the Schottky equation,

$$\log J_{RS} = \log J_R + \frac{1.912}{T}\sqrt{E}$$

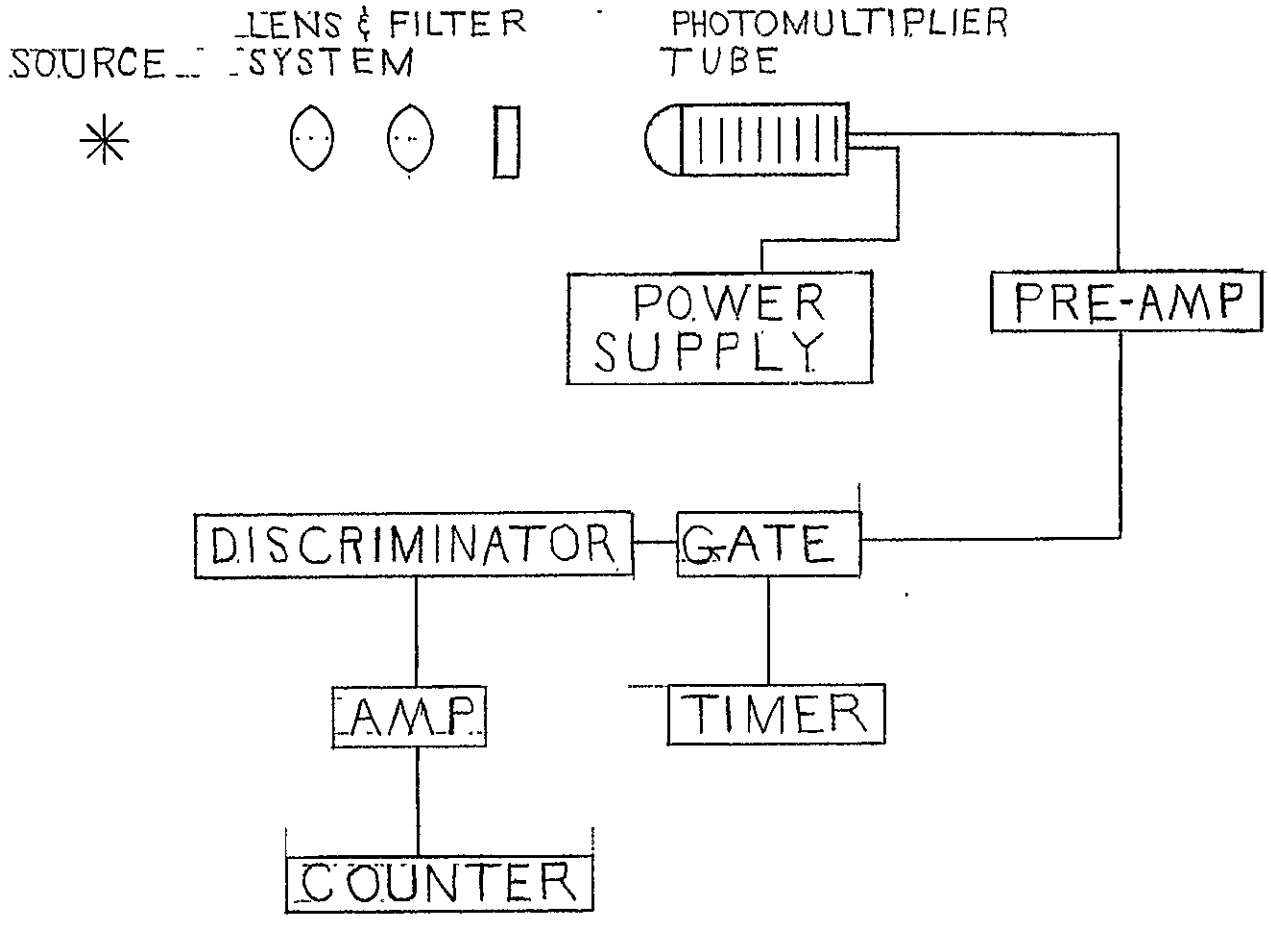

FIG 6: PHOTON COUNTER SCHEMATIC

J_R is the zero field Richardson current, J_{RS} is the Schottky current, and E is the electric field. The plot of log J_{RS} vs $\sqrt{E}$ can be extrapolated to determine J_R. J_R can then be substituted into the Richardson-Dashman Equ. and the effective work function can be calculated. Fig. 7 is presented for completeness and typifies the Schottky plots generated during this work.

Since the electric field is a parameter in the work function determination, the sample (emitter) to collector spacing was determined with precision as a function of temperature by a positive emitter-collector electrical short method.

III. Superalloy Materials

1) Selection

A number of nickel base superalloys, those listed in Tables 1 were potential candidates for low temperature thermionics. The suggested materials have high temperature capabilities for operation in an oxidizing atmoshpere. Some of these specifics for each of the materials are indicated in Table 1, including machinability, the high temperature capability of the materials, use conditions, forging temperature, material availability, and some specific current uses. The machinability will is very important as a cost consideration, especially for large scale diode production. Since the diodes will probably be operated in air on a combustion atmoshpere, the material must withstand oxidation and other corrosions. The nominal temperature limits are stated for each of the seven candidates. Many other important properties were not included in Table 1.

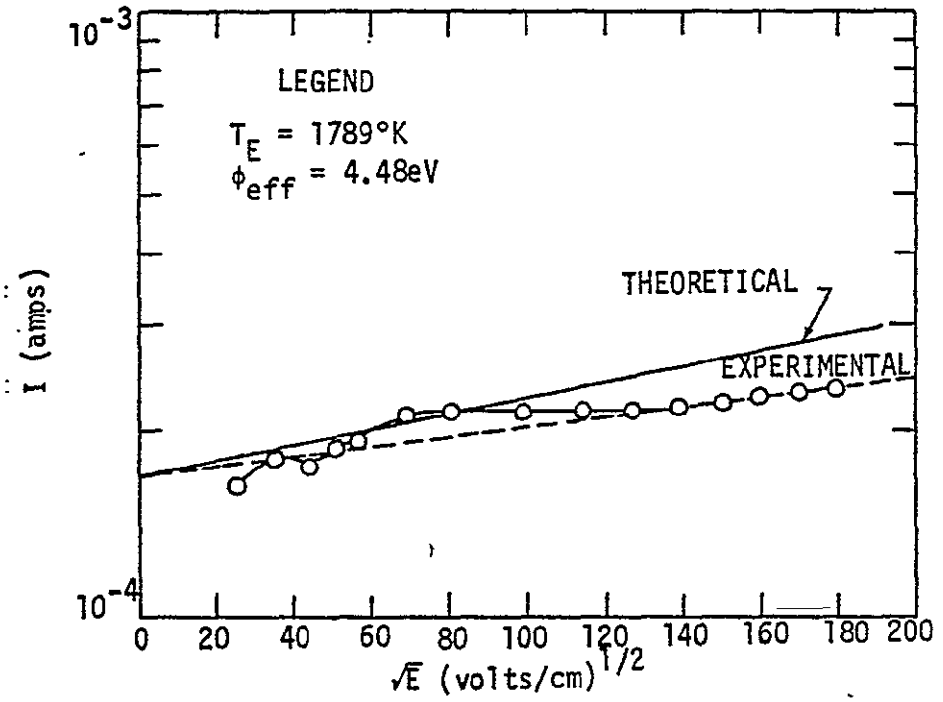

Figure 7. Schottky Plot of Polycrystalline Molybdenum Sample Determined from Vacuum Emission Vehicle Measurements.

Table 1 GENERAL PROPERTIES OF NICKEL-BASED SUPERALLOYS

	HASTELLOY-B	HASTELLOY-X	HASTELLOY-S	INCONEL 600	INCONEL 617	INCONEL 718	INCONEL X-750	INCOLOY 800	RENE 41	WASPALOY	L-605
Composition (%)											
C	.05	.1	.02	.08	.07	.08	.04	.1	.09	.1	0.15
Mn	1.0	.5	.2	.5	-	.35	.7	1.5	-	.5	-
Si	1.0	.5	.2	.25	-	.35	.3	1.0	-	.5	-
Cr	1.0	22.0	15.5	15.5	22.0	17-21	15.0	19-23	19.0	19.5	20.
Ni	64-51.45	47.3	67.35	76.0	54.0	50-55	74.0	30-35	55.3	55.0	10.
Co	2.5	1.5	15.5	-	12.5	1.0	-	-	11.0	13.5	51.85
Mo	26-30	9.0	-	-	9.0	2.8-3.3	-	-	10.0	42.5	-
W	-	.6	-	-	-	-	-	-	-	-	15.
Cb	-	-	-	-	-	-	.9	-	-	-	-
Ti	-	-	-	-	-	.65-1.15	2.5	.15-.60	3.1	3.0	-
Al	-	-	.2	-	1.0	.20-.80	.08	.15-.6	1.5	1.3	-
B	-	-	.009	-	-	-	-	-	.01	.005	-
Zr	-	-	-	-	-	-	-	-	-	.085	-
Fe	4-7	18.5	1.0	8.0	-	Remainder	6.8	Remainder	-	2.0	.3
Other	-	-	.02	.25	-	5.8	-	.765	-	-	
Density (gm/cm^3)	9.25	8.23	8.75	8.34	8.36	8.2	8.25	7.95	8.25	8.2	9.25
Melting Range (°C)	1301-1368	1287	1335-1380	1354-1413	1332-1377	1260-1336	1343-1427	1360-1385	----	----	
Specific Heat (70°F) [Joule/kg-°C]	379	483	395.5	441.3	417	433	429	500	458	417	410
Thermal Conductivity [$Watt/m^2$-°C]											
21°C	40.14	-	45.81	47.51	44.23	36.4	39.23	37.8	-	-	-
600°C	53.86	68.04	85.5	78.25	73.14	66.15	-	67.6	-	-	-
870°C	-	43.66	-	94.69	87.32	81.75	77.51	85.5	82.78	82.78	-
Coef. of Thermal Exp. [10^6 cm/cm °C]											
93°C	-	13.86	11.52	13.32	11.52	12.96	12.53	14.22	-	-	-
870°C	14.04	16.38	14.76	16.38	15.66	17.1	16.79	18.36	16.74	17.46	-
Elec. Resistivity (75°F) [$\frac{10^{-6}\ Ohm}{cm}$]	135	118.3	-	-	-	1.25×10^{-6} r-cm	-	9.89×10^{-5} r-cm	-	-	-

TABLE 1

GENERAL PROPERTIES OF NICKEL-BASED SUPERALLOYS (Cont'd)

	HASTELLOY-B	HASTELLOY-X	HASTELLOY-S	INCONEL 600	INCONEL 617	INCONEL 718	INCONEL X-750	INCOLOY 800	RENE 41	WASPALOY	L-605
MODULUS OF ELASTICITY [10^6 psi]											
Room Temp.	26.4	28.5	30.8	31.4	-	29.0	31.0	28.35	31.8	31.9	34.2
540°C	29.6	23.8	26.4	27.1	-	24.8	26.7	23.43	-	-	-
815°C	21.8	-	-	-	-	21.3	-	20.60	24.2	24.5	-
ULT. TENSILE STRENGTH [ksi]											
Room Temp.	134.	113.	116.	90.	110.	180.	162.	85.5	206.	188.	130.
540°C	113.	94.	84.9	84.	86.	-	140.	73.7	-	-	-
815°C	-	-	-	28.	50.	-	-	-	126.	100.	-
YIELD STRENGTH [ksi] (.2% off)											
Room Temp.	56.5	52.2	48.7	36.	48.	-	92.	36.2	154.	120.	59.
540°C	39.3	41.5	24.	28.	31.	150.	84.	25.8	-	-	-
815°C	-	-	-	-	31.	-	-	-	118.	90.	-
HARDNESS-BRINELL											
25°C	205.	-	-	120-170	-	331 BHN	-	138	-	-	-
540°C	156.	-	-	-	-	-	-	90	-	-	-
RUPTURE STRENGTH (1000 hr, 1000 psi)											
650°C	36.5	43.0	43.0	-	47.	80.	68.	20.	102.	-	-
815°C	9.4	11.5	11.5	8.2(1400°F)	16.	-	16.	3.6	29.	-	-
OXIDATION RESISTANCE (°C)	760	1200	1150	1100	----	-	1050	-	1000	950	1055
HOT WELDING TEMP (°C)	1000-1200	1000-1200	815-1150	870-1250	1000-1200	1065	1000-1200	540	1000-1175	1000-1175	
MACHINABILITY	a	a,b	-	c	-	-	d	-	h	c,e	c
WELDING	a,i	f	-	f	k	-	g	-	-	-	f

a. Similar to austenitic stainless steels.
b. Low cutting speeds required.
c. Hi-speed steel of carbide tools required.
d. More difficult than austenitic stainless steels.
e. Grinding required for finishing.
f. Resistance, fusion, brazing.
g. Fusion difficult.
h. Gummy, must be aged; tungsten carbide tools required.
i. Oxyacetylene not recommended for corrosion applications.
j. Should occur in annealed condition, w/minimum heat input.
k. Weldable by conventional techniques.

Table 1 shows, for comparison sake, the ultimate tensile strength, the tensile yield strength, the tensile modulus, and the coefficient of expansion for the seven materials as a function of temperature.

Table 2 gives the nominal compositions of the candidate materials plus some for comparison.

The nickel base alloys have high toughness, good workability, and high temperature oxidation resistance in general. Some of the alloying additions include cobalt, iron, chromium, molybdenum, titanium and aluminum. Cobalt contributes to the high temperature strength; iron tends to strengthen the nickel matrix and is cheaper than nickel; chromium enhances strength and oxidation resistance at high temperatures; molybdenum contributes to the solid solution strengthening; and titanium and aluminum are primarily agents which permit precipitation hardening of the alloys.

It should be noted that a number of the materials will not withstand sulfur atmospheres. At high temperatures sulfur can cause embrittlement of the material and lead to failure.

A number of the materials tend to cold work very easily, and this can complicate the required machining procedures. Some of the materials need to be annealed frequently during material removal operations. Most of the materials can be welded and brazed, and specifications for these procedures exist for all the materials listed. Age hardening conditions for the age hardenable materials are also specified.

After evaluating the materials in regard to literature properties a number of superalloys were chosen for testing. The list is as follows:

Table 2 COMPOSITIONS OF ALLOYS STUDIED FOR THERMIONIC ELECTRODES AND/OR FOR NA CORROSION CHARACTERISTICS

	Nominal Composition, %														
Alloy	C	Mn	Si	Cr	Ni	Co	Mo	W	Cb	Ti	Al	B	Zr	Fe	Other
Incoloy 800	0.05	0.75	0.50	21	32.5	--	--	--	--	0.38	0.38	--	--	46	--
Refractaloy 26	0.03	0.8	1.0	18	38	20	3.2	--	--	2.6	0.2	--	--	16.2	--
Haynes alloy 188 (sheet)	0.08	--	--	22	22	Bal	--	14	--	--	--	--	--	1.5	0.08 La
Hastelloy alloy C	0.08	1.0	1.0	15.5	54.6	2.5	16.0	3.8	--	--	--	--	--	5.5	--
Hastelloy alloy N	0.08	0.8	1.0	7.0	67.9	0.2	16.5	0.5	--	--	--	0.01	--	5.0	0.5 Al + Ti
Hastelloy alloy X	0.15	1.0	1.0	21.8	45.5	2.5	9.0	0.6	--	--	--	--	--	18.5	--
Inconel 601	0.05	0.5	0.25	23	60.5	--	--	--	--	--	1.35	--	--	14.1	0.25 Cu
Inconel 617	0.07	--	--	22.0	54.0	12.5	9.0	--	--	--	1.0	--	--	--	--
Inconel 718	0.04	0.20	0.30	18.6	52.9	--	3.1	--	5.0	0.9	0.4	--	--	18.5	--
René 41	0.09	--	--	19	55.3	11	10	--	--	3.1	1.5	0.010	--	--	--
TAZ-8A	0.125	--	--	6.0	68.4	--	4.0	4.0	2.5	--	6.0	0.004	1.0	--	8.0 Ta
TAZ-8B	0.125	--	--	6	64.4	5.0	4.0	4.0	1.5	--	6.0	0.004	1.0	--	8.0 Ta
TRW VI A	0.13	--	--	6	61.6	7.5	2.0	5.8	0.5	1.0	5.4	0.02	0.13	--	9.0 Ta, 0.5 Re, 0.43 Hf
WAZ-20	0.15	--	--	--	73.7	--	--	18.5	--	--	6.2	--	1.5	--	--
Stainless Steel 304	0.08	2.0	1.0	19	10	--	--	--	--	--	--	--	--	67.8	0.045 P, 0.030 S
Stainless Steel 316	0.08	2.0	1.0	17	12	--	2.5	--	--	--	--	--	--	65.5	--

Inconel 601	WAZ 16
Inconel 718	WAZ 20
Inconel 617	NASA-TRW Alloy VI A
Incoloy 800	TAZ 8A
Hastelloy X	TAZ 8B
L-605	VM 108

2) Sample Configuration

The form of the metals received for sample fabrication varied from sheet to billet. For the purposes of this project, it was decided that the billet form would be of the most utility. The samples were fabricated by machining a hole in the billet, leaving a flat disc emitter supported by an integral heat choke. A hohlraum was also machined in each disc.

A rough approximation for (t) and (L) for the cylinder was obtained by assuming that the energy radiated from the surface of the cylinder is equal to the energy conducted down the sides of the cylinder.

$$q_{cond.} \doteq q_{rad}$$

$$-k[\pi(r + t)^2 - \pi r^2] \frac{\Delta T}{\Delta x} \doteq \sigma\varepsilon 2 (r + t) L (T^4 - T_\infty^4)$$

where r = radius of cylinder

but $t \ll r$

$$\therefore \; -k2\pi rt \frac{T_2 - T_1}{L} \doteq \sigma\varepsilon 2\pi rL(T^4 - T_\infty^4)$$

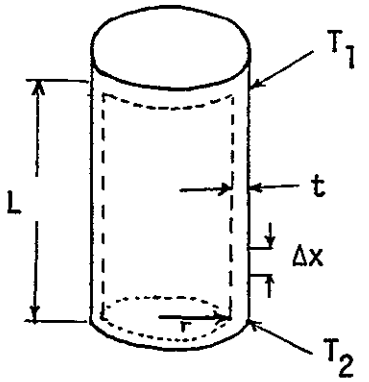

Let T = average temperature of cylinder surface

$$T \doteq \frac{T_1 + T_2}{2}$$

$$T^4 \gg T_\infty^4$$

$$\therefore \; k2\pi rt \frac{T_1 - T_2}{L} \doteq \sigma\varepsilon 2\pi rL\left(\frac{T_1 + T_2}{2}\right)^4$$

$$L \doteq \sqrt{\frac{16kt(T_1 - T_2)}{\sigma\varepsilon(T_1 + T_2)^4}}$$

To solve for L use values for stainless steel and let T_1 - 1700°K, T_2 = 1000°K.

The sides of the cylinder act as a heat choke so (t) should be made as small as possible but not so small as to make the structure weak.

So let (t) = 50 mills

with these values then:

L ≐ .5 inches.

It is intended that the optimal (L) be perimentally determined through comparison with results obtained for stainless steel samples of varying (L).

3) Mass Spectrometer Evaporation Measurements for Incoloy 800.

Two problems were encountered in making vacuum emission measurements. The first involves the very high vaporization rates of some of the elements of which the alloys fabricated. The second involves the very low current densities which are obtainable from these materials in the temperature range of interest, 1000°K to 1400°K. The vaporization problem has been identified and discussed by Mr. Jim Morris at Lewis Research Center at the National Thermionics Meeting and also in informal discussion. The experience in this laboratory is that above 1200°K, very heavy desposits of evaporated material have been found on the collector and guard ring. A few selected super alloys have been sent to LASL for examination in the mass spectrometer. In this examination the samples were held at the operational temperature while an evaluation is made by mass spectrometry of the elements which are being evaporated and the rate at which they are being evaporated.

The Incoloy 800 has been evaluated in the mass spectrometer. Vapor species between mass 24 and 80 were measured. In this range, Cr, Mn, Fe, Ni and Cu were found to be present in the vaport. The composition of Incoloy 800 is given in Table 2. C, Si, Ti, and Al have mass numbers less than 24. Cu appears, apparently as an impurity. The percent of total pressure after various heating times is given at two interpolated temperatures in Table 3. Measurements were made between 1300°K and 1547°K.

Table 3. Mass Spectrometer Determination of Vapor Composition of Incoloy 800.

Vapor Composition: % of total pressure

		Initial		
T°K	Cr	Mn	Fe	Ni
1300	46	45	9	-
1500	56	15	28	-
		Heated at ∿ 1525K for 144m		
1300	48	31	21	-
1500	45	9	45	+ trace Ni and Cu
		Heated > 1600K for 35 h		
1300	54	18	25	3
1500	50	7	36	7

Evaporation at high temperatures tends to produce a surface which is richer in Ni and poorer in Mn than the bulk material. Also the surface will become richer in Fe compared to Cr. The total pressure decreases as evporation proceeds. The amount of Ni being lost is lower than would be expected relative to pure element vapor pressure charts. The Ni appears to be bound tight in the lattice, possible partly with Al and one of the

other lighter elements. Further analyses on the other mentioned alloys will continue in order to try to obtain more complete trends.

The spectrometer was calibrated with Fe and the resulting activities are plotted in Figures 8 and 9. The behavior of Fe can be treated, but the absolute activities of Mn, Cr and Ni are less certain, although the temperature variations should be accurate. Apparently, the activity of Fe is unity below 1430°K and drops rapidly above this temperature. Since other components behave in a similar way, compound formation may occur at a higher temperature, or a strongly enhanced mutual soluability may exist.

From activity, the evaporation rate can be calculated for the various alloy components and compared to the elements as a function of temperature. Time is also an important parameter since a given component can be continually removed in a selective manner resulting in an alloy with a changing bulk composition. It can be seen for example in Fig. 10 that the Mn is considerably below the elemental evaporation at that temperature.

4) High Temperature Properities of Some Super Alloy and Other Alloys

Thermionic topping of large power installations such as a conventional steam power plant will probably require the use of relatively low cost materials. With this in mind super alloys and relatively low cost carbides and borides are being evaluated for electrode applications. The vapor pressure problem was discussed in the last section. The high temperature (1400°K) predicted for such applications also demands that the strength and corrosion characteristics of the electrodes be suitable for long life. A number of strength characteristics are examined in the next subsection. The electrodes will probably be exposed to alkali metals, cesium on the convertes side, and possible a heat transfer medium such as sodium on the opposite side. For economy and manufacturing convenience, it would

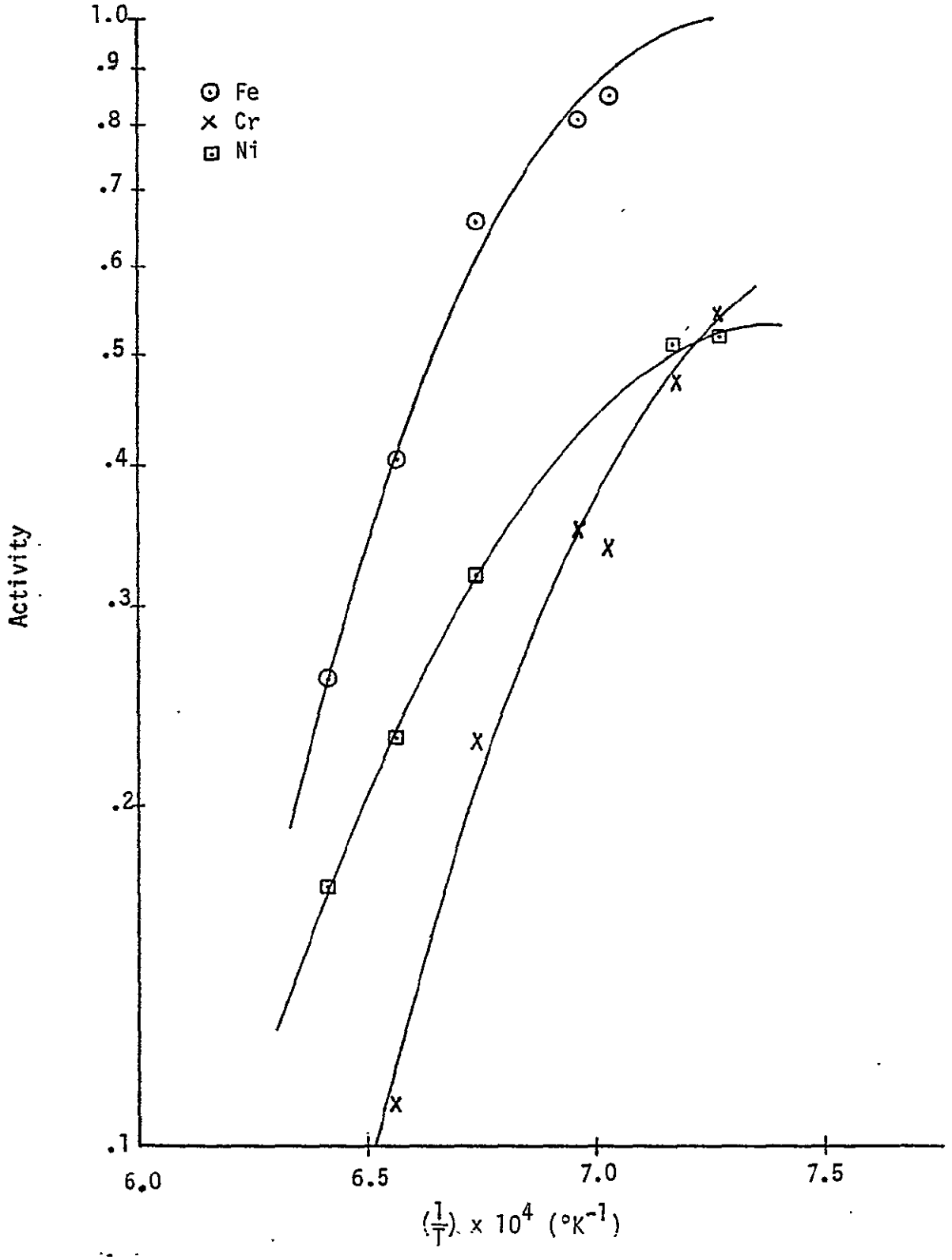

Figure 8. Activity v.s. Temperature for Incoloy 800 after 35 hours at 1600°K.

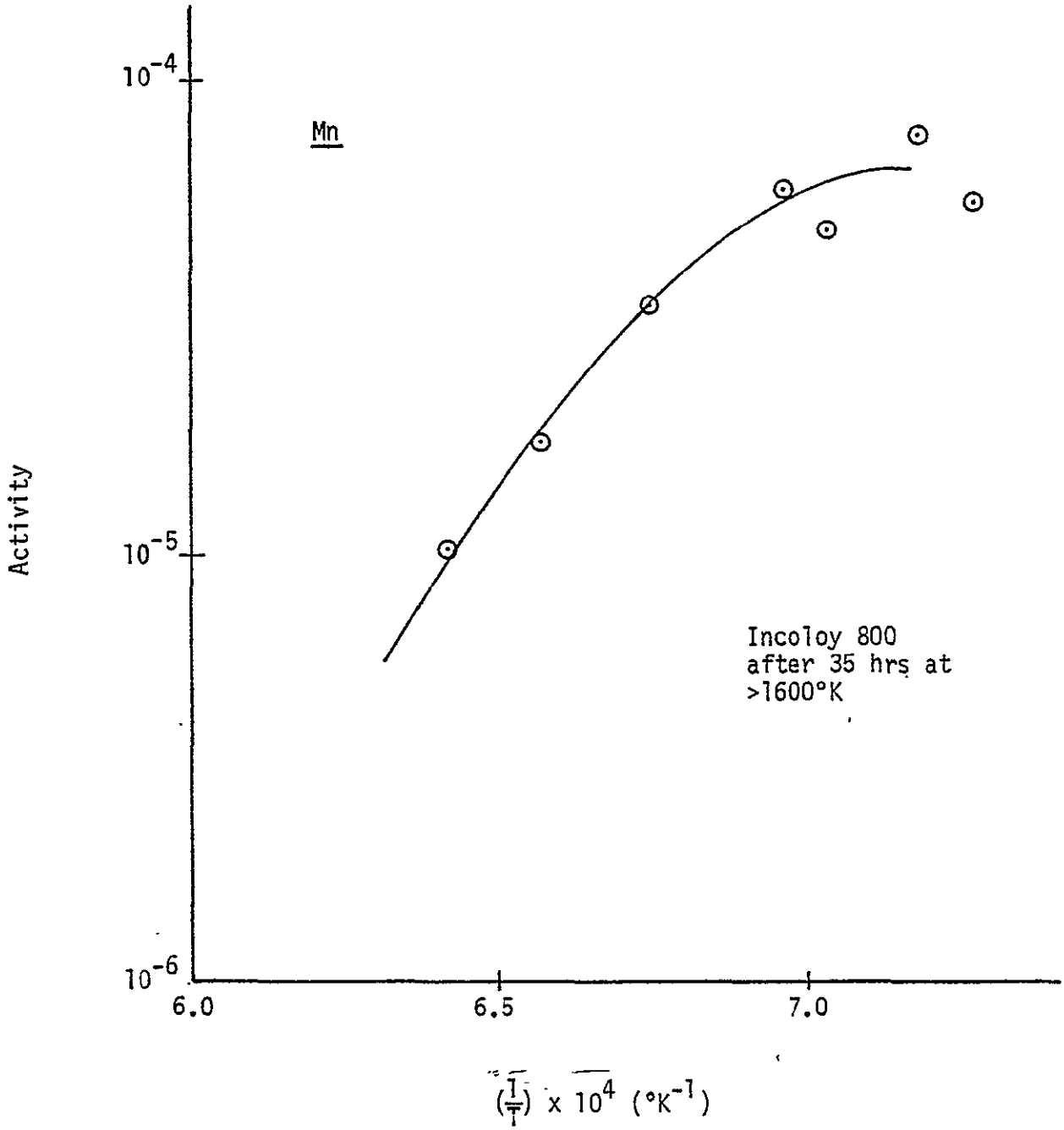

Figure 9. Activity v.s. Temperature for Incoloy 800 after 35 hours at 1600°K.

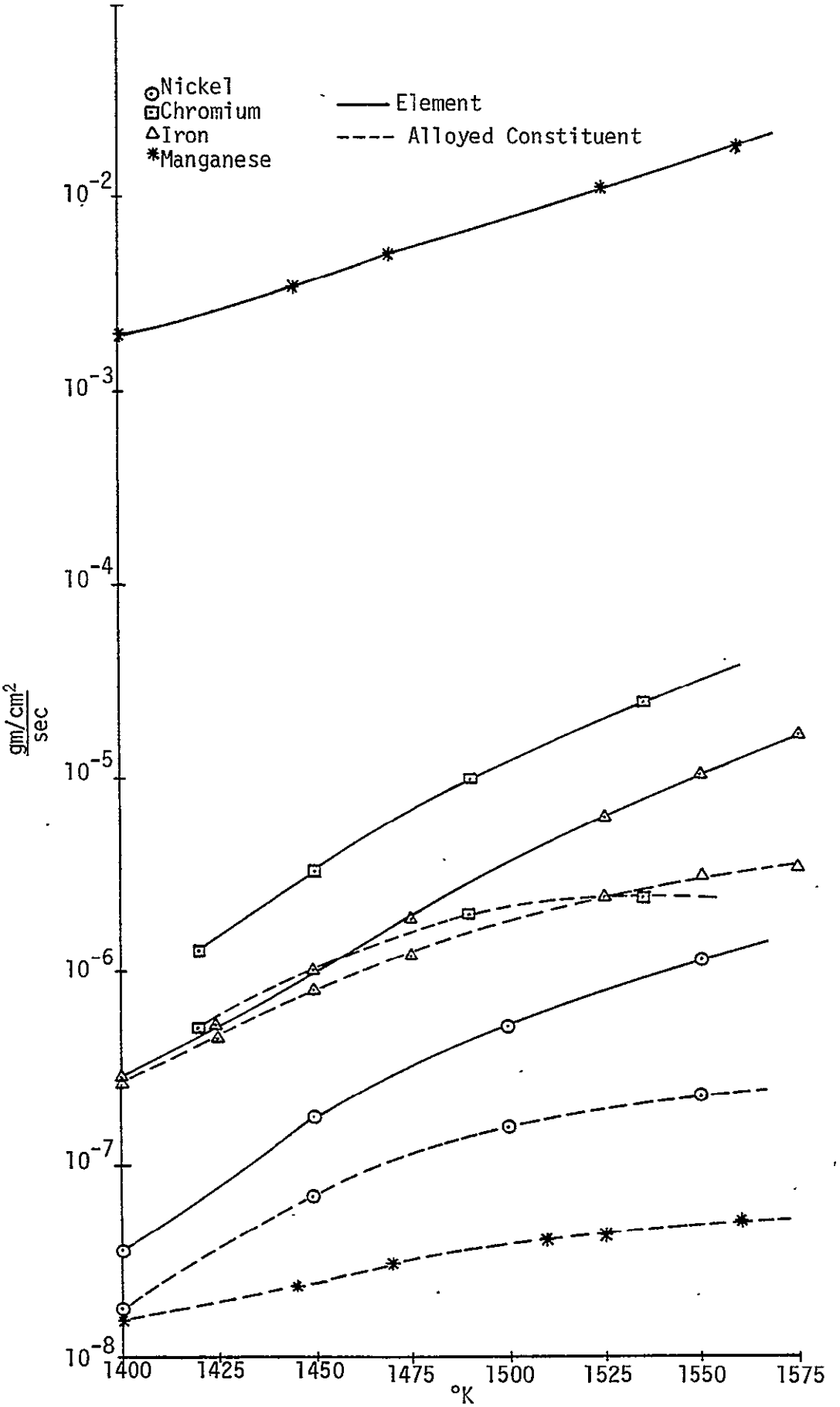

Fig. 10. Evaporation of Alloy Constituents from Inconel 800 After Heating For 35 hr > 1600°K

be desirable to have a single material for the heat transfer medium and for the emitter. This would also be true on the collector side. In subsection the compatibility of the selected alloys will be evaluated, primarily with sodium. Extensive literature is available regarding the compatibility of sodium with some materials, primarily austenitic stainless steels. These results have been obtained for the Liquid Metal Fast Breeder Reactor programs. Stainless steels have been tentatively selected for the heat transfer loops with sodium, but because of the limited strength at predicted high temperature applications, super alloys are now being promoted and entered into the strength and corrosion experiments being conducted in a number of laboratories.

5) High Temperature Mechanical Properties

Tables 4 and 5 list a number of mechanical properties for the alloys, at 1000°K in Table 3 and at 1400°K in Table 5 except where data at other temperatures is specifically noted. Comparisons are difficult in many cases because the conditions of data acquisition are not exact. Relative values of strength can be seen in many cases though. Rene 41, the TAZ, TRW, WAZ and Refractalloy 26 alloys have superior high temperature mechanical properites. Some considerations such as the fabrication techniques applicable to these materials are important for practical applications. TAZ, WAZ and TRW alloys contain a reasonable percentage of tungsten, and are formed by arc melt castings. These materials along with Haynes 188 and Refractalloy 26 are difficult to machine and must be ground or electron discharge machined in many cases. The Inconel and Hastelloy series are more amenable to cost effective machining.

The overall strength characteristics of the alloys must be matched to the expected loads in the system and designed to minimize cost. Creep

Table 4 NOMINAL ELEVATED TEMP. STR. OF CONTAINMENT ALLOY AT 1000°K

Alloy	Tensile Strength MN/m^2	Yield Strength MN/m^2	Stress-to-rupture in 1000 hr. MN/m^2	Creep Strength 1%, 1000 hr. MN/m^2
304 S.S.	207	138	21	8
316 S.S.	207	138	55	19
Hastelloy C	448	276	172	
Hastelloy N	386	203	35	
Hastelloy X	345	207	69	51
Inconel 601	379	172	83	
Inconel 617	414	166	193	35
Inconel 718	724	689	593	97
Rene 41	896	772	345	128 @ .2% 100 hrs.
TAZ 8A	896			
TAZ-8B	980			
TRW VIA			655	
WAZ-20				
Incoloy 800	241	166	41	38
Haynes 188	552	283		93
Haynes 25	345	241	117	62
Refractaloy 26	689	620	207	255
Nickel 270	48	17		35 @ 1% 1000 hrs.

Table 5 NOMINAL ELEVATED TEMP. STRENGTH OF CANDIDATE ALLOYS AT 1400°K

Alloy	Tensile Strength MN/m^2	Yield Strength MN/m^2	Stress-to-rupture in 1000 hr. MN/m^2	Electrical Resistivity Micro-ohm-cm	
				293°K	1400°K
304 S.S.	62 (1300°K)	69 (1200°K)	10 (1300°K)	75	
316 S.S.	35	138 (1200°K)	8 (1300°K)	74	
Hastelloy C	110		35 (1250°K)	129	
Hastelloy N	235 (1250°K)	179 (1250°K)			
Hastelloy X	69	69	6	118	
Inconel 601	35	35	7	119	130
Inconel 617			11		117
Inconel 718	69	69		124	135
Rene 41	276 (1300°K)	262 (1300°K)	138 (1250°K)		
TAZ 8A	55		66 (100 hr.)		
TAZ-8B	83		79 (100 hr.)		
TRW VIA			55		
WAZ-20			79 (100 hr.)		
Incoloy 800			10 (1255°K)	99	131
Haynes 188	138		15 (100 hr.)	92	
Haynes 25	83	83	28 (1255°K)	87	100 (1361°K)
Refractaloy 26	276 (1300°K)	276 (1300°K)			
Nickel 270	28 (1255°K)	14 (1255°K)		16	51

strength is very important for long term applications, and at 1400°K, little creep data is available for many of the mateirals.

6) Alkali Metal Corrosion

The alkali metal environment must be evaluated for a number of different corrosion phenomenon.

- dissolution of containment (leaching)
- embrittlement (grain, grain boundary)
- mass transfer
- erosion (flow velocity dependence)
- electrochemical
- galvanic (dissimilar metals)
- precipitation inducement
- stress corrosion

Some important parameters influencing some of the above mechanisms are:

- maximum system temperature
- maximum temperature differentials
- alkali metal oxide levels (and other impurities)
- alkali metal flow velocity
- heat flux

As stated considerable information is available for some stainless steels. A summary of some static corrosion tests in sodium is presented in Table 6. In static systems the corrosion appears to be limited, although the test duration of 400 hr. is not very substantial. The sodium corrosion of austenitic stainless steel for pumped loop experiments is given in Table 7. A verbal summary for 316 s.s. and for 304 s.s. from the experiments is that they can be used up to 805°K in sodium flow, provided

Table 6 STATIC CORROSION IN SODIUM, 400 hr., 1273°K

METAL	INTERGRANULAR PENETRATION mm	SUBSURFACE VOIDS mm	DECARBURIZATION mm	GENERAL CORROSION
304 S.S.	0.000	0.076	--	Some surface voids
316 S.S./ 347 S.S.	0.000	0.051	0.102	Some surface voids
Inconel	0.000	0.013	0.025	Very shallow attack
80 Ni - 20 Cr	0.000	0.000	0.000	None observed
Nickel	0.000	0.000	0.000	None observed

Table 7 SODIUM CORROSION OF AUSTENITIC STAINLESS STEEL FROM LITERATURE (DATA)

(Pumped Loop Experiments)

SITE	MATERIAL	T_{max} °K	ΔT °K	V m/sec	Ox. ppm	TIME	CORROSION
G.E.	347 S.S.	660	(2)	∿3	220	3 years	None
LASL	316 S.S.	866	134	∿1.5	Low	18 months	T.S., Hardness increase
Babcock & Wilson	304 S.S.	866	0	∿17	Low	1,000 hrs.	Little attack
Babcock & Wilson	316 S.S.	866	0	∿17	Low	1,000 hrs.	Little attack
G.E. Vallecitos	316 S.S.	866	134	∿9	10	30,000 hrs.	Weight loss, intergranular penetration, carbon transport, surface transformation.
Soviet	18 Cr	894	--	--	Var.	5,500 hrs.	Corrosion attack; mechanical property changes.
ORNL ORNL ORNL	316 S.S. 304 S.S. 347 S.S.	1089 1089 1089	166 166 166	-- -- --	-- -- --	1,000 hrs. 1,000 hrs. 1,000 hrs.	Intergranular penetration 0.051 to 0.127 mm. Little mass transfer for 316, 304, and 347.
ORNL	310 S.S.	1089	166	--	--	1,000 hrs.	Intergranular attack, void formation to 0.330 mm, cold zone deposits.
ORNL	316 S.S.	1171	166	--	--	1,000 hrs.	Hot zone intergranular attack to 0.051 mm, small voids to 0.127 mm, cold zone deposit 0.076 to 0.127 mm thick.
ORNL	316 S.S.	1660	--	--	20 30	1,000 hrs.	Hot zone surface attack to 0.076 mm. $\gamma \rightarrow \alpha$ transformation to 0.012 mm. Cold zone deposits.

Table 8 SODIUM CORROSION OF Ni and CO BASED ALLOYS
FROM LITERATURE (DATA)
(flow systems)

MATERIAL	T_{max} °K	Time hr	ΔT °K	CORROSION
Hastelloy X	1088	1000		None
Hastelloy X	1200	305	361	Hot zone attack, voids intergranular attack
Inconel	1088	1000	167	Hot zone attack, 0.051 mm Heavy cold zone deposits
Hastelloy W	1088	1000		Ni deposits in cold zone

Table 9 SODIUM HEAT PIPE PERFORMANCE FROM LITERATURE

MANUFACTURER	CONTAINMENT MATERIAL	OPERATING TEMPERATURE	OPERATING TIME (HRS.)	FAILURE MECHANISM
Dynatherm	304 S.S.	923°K	16,500	None
RCA	304 S.S.	1073°K	7,200	--
Xerox/EOS	304 S.S.	1000°K	~4,000	None
Hughes	304 S.S.	923°K	2,380	--
LERC	304 S.S.	1000°K	--	--
RCA	316 S.S.	1044°K	4,000	--
RCA	(A) Nickel	1073°K	20,000	None
RCA	Hastelloy X	988°K	20,000	--
RCA	Hastelloy X	988°K	8,000	--
BROWN-BOVERI	Nb - 1% Zr	1000°K	28,000	Two leaks (fixed)
LERC	Nb - 1% Zr	1000°K	3,000	--

Table 10 RELATIVE CORROSION OF AUSTENITIC STEELS AND SUPER ALLOYS

ALLOY	T °K	VELOCITY	LIFE	(Impurities) OXYGEN	GENERAL ATTACK	STRENGTH
304, 316, 347	850	High	Unlimited	Limited to few ppm	Minimum	Good
304, 316, 347	850 to 950	High	Dependent	Limited to few ppm	Moderate	Moderate
304, 316, 347	1050	Low	Limited	Limited	High	Poor
Super alloys (Ni Based)	<1000	Low	Good	Low	Low	Good
Super alloys (Ni Based)	>1000	Medium	Limited	Low	Several times greater than for stainless Ni leaching	Reduced
Super alloys	950 to 1100	Low	Limited	>20 ppm	Decarburization	Reduced creep strength
Super alloys	950 to 1100	Low	Long	Few ppm	Low attack as long as Oxygen content is low	Good

that the oxygen and carbon impurity levels in the sodium are kept low. Transfer of interstitial elements to and from sodium exposed austenitic surfaces is possible in systems being considered here. When austenitic and ferritic steels are commonly exposed to the sodium environment migration of carbon can occur resulting in a decrease in strength of the carbon depleted material while embrittling the carbon rich system. In a pure 304 s.s., sodium flow system, acceptable performance appears to be obtainable as long as the oxygen level in the sodium is maintained to a few parts per million. 316 s.s. has charactertistics similar to 304 s.s. Table 7 provides some data from various experiments.

Table 8 provides some data from the literature for sodium corrosion of super alloys. Except at the low temperature, 1088°K with no ΔT, corrosion appears. They oxygen level was not available in these experiments nor were the exact flow rates.

Table 9 summarizes some sodium heat pipe results from the literature. The oxygen contents of the sodium, and flow rates were again not available. The reports indicate that in most cases, the heat pipes did not fail. The studies in general, do not report post test analyses to provide data on corrosion that has taken place. Thus, it is impossible in most cases to make any predictions for long term behavior. Since heat pipes are important candidates for many thermionic applications, it will be necessary to obtain mroe reliable corrosion data in order to design practical systems for long term reliable use.

Table 10 is a summary based upon a general culmination of literature corrosion studies and a qualitative prediction of behavior with temperature, flow rate and oxygen impurities as parameters.

IV. Transition Metal Alloys

A second objective of the work was accomplished in conjunction with Los

Alamos Scientific Labs. A study of a class of materials which have a demonstrated application to very high temperature problems was performed. These are the transition metal borides, borocarbides, and boronitrides. Emphasis was given to that behavior which must be known regardless of the application. The general theme was to determine how the properities can be modified and to what extent. There are three general properties which limit the usefulness of a material at very high temperatures. Properties related to strength, transport properties which include diffusion and vaporization rates, and reaction rates with other materials or gases in the environment. Measurements were made of the chemical activity and the vapor pressure of the component elements was calculated and determined as a function of composition. A special high temperature mass spectrometry system has been developed and tested for making these measurements at Los Alamos.

The intent of this work was and remains is to find the basic relationships between diffusion, work function and bond energy. The materials to be studied eventually involve binary and ternary systems of the transition metal borides and carbides will be considered for application to thermionics. The overall application of these materials as electrodes for thermionic energy converters is determined.

Preliminary work in Russia and Germany has shown that the class of materials to be studies have work functions which can be modified over a wide range. This, combined with good stability at high temperatures, opens new possibilities for the design for more efficient thermionic diodes by combining measurements of the vaporization behavior with maintenance of the work function using the same samples. This provides the unique position, not only to answer immediate practical questions, but to study the relationship between these basic properties.

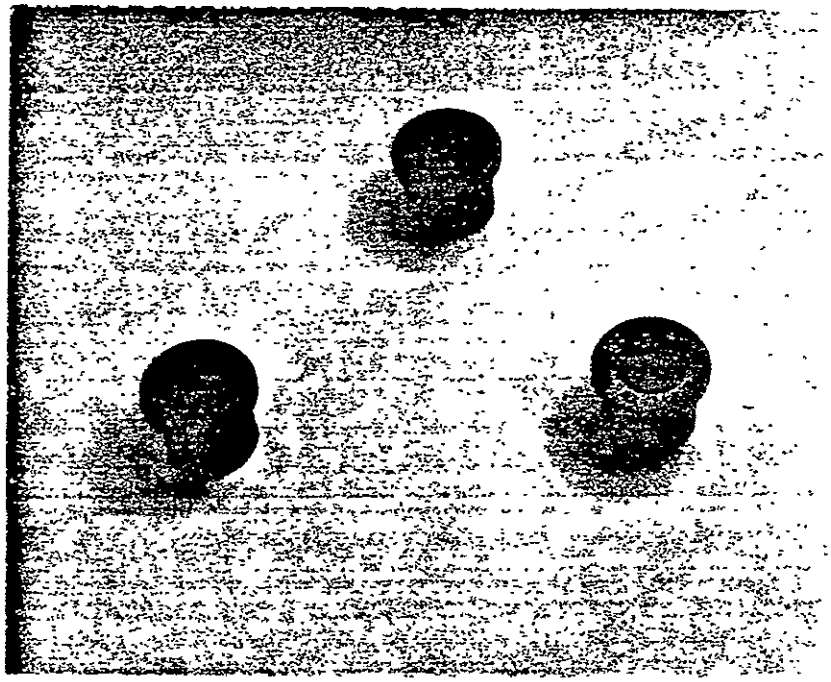

Figure 11

WORK FUNCTION MEASUREMENT OF LANTHANUM — BORON COMPOUNDS*

D. L. Jacobson
Arizona State University
and
E. K. Storms
Los Alamos Scientific Laboratory
Received July 18, 1977

ABSTRACT

The La-B system was studied between $LaB_{4.24}$ and $LaB_{29.2}$, and between 1400 and 2100 K to determine the phase relationship, the chemical activity of the components, the vaporization rate and the vapor composition.

A blue colored phase near LaB_9 was found to exist between purple colored LaB_6 and elemental boron.

Diffusion is so much slower than vaporization that large composition differences can exist between the surface and the interior which, nevertheless, produce a steady state loss rate from freely vaporizing material. The flux at 1700 K is 6×10^{-10} g/cm^2-sec for $LaB_4 + LaB_6$ and 7×10^{-11} g/cm^2-sec for $LaB_6 + LaB_9$. There is an activation energy which lowers the vaporization rate of boron from LaB_6. Freely vaporizing material will have a steady state surface composition between $LaB_{6.04}$ and $LaB_{6.07}$, depending on temperaure, purity and interior composition.

The free energy of formation of LaB_6 is (0.071T-351) kJ/mole between 1700 K and 2100 K.

INTRODUCTION

Multicomponent materials such as the Rare Earth compounds of lanthanum (La) and boron (B) for thermionic emitters has brought about a need for increased understanding in the relationship between work function and alloy composition. In the past when pure metals were used for thermionic emitters, it was required only to know the work function and its dependence on temperature, purity, surface preparation and sometimes grain orientation. Emission characteristics of alloys are strongly dependent upon surface composition which is in turn dependent upon a number of other factors including temperature, initial bulk composition, density and the relationship between bulk diffusion rate and evaporation rate. The dependence of the work function on these parameters can result in emission properties which change with time as the sample obtains equilibrium conditions at a given temperature.

The objective of the work reported in this paper is to begin to demonstrate a relationship between emission properties and sample composition under equilibrium conditions. The emission properties measured in this work are correlated with surface composition. The relationships among the pertinent properties will eventually be demonstrated such that one can choose conditions which will lead to a stable long life electrode system.

In the present program the binary compounds of La and B are being investigated in order to establish the equilibrium long life conditions under which it will perform as an efficient emitter. The samples are being prepared by cold pressing and sintering in a manner similar to that which would probably be used for commercial electrodes. Other properties pertinent to the thermionic capabilities of these materials are being investigated when possible. Present work in the binary compounds of La and B are intended to be the foundation for more advanced compounds, probably of a ternary nature which are intended to allow for lower vaporization rates and lower work functions. The ultimate life of a thermionic diode depends upon the vaporization rate of the electrodes, while the efficiency is a function of the electrode work function.

* This work was partially under NASA Grant NSG 7019 through NASA Lewis Research Center.

EXPERIMENTAL

Apparatus

The gemoetry of the vacuum emission vehicle is shown in Figure 1. It consists of an emitter sample, an electron bombardment heater assembly, a collector, and a guard ring. Samples rest on tantalum heat choke assembly. The sample is heated directly either by radiation or by electron bombardment from a pancake type counterwound tungsten filament inside the heat choke cavity.

Sample temperatures are measured with a micro-optical pyrometer which is focused on a 10 to 1 hohlraum located in the side of the sample and parallel to the emitting surface. The molybdenum collector and guard ring are mounted parallel to the sample at a spacing of approximately 0.1 cm. The electron emission from the central 1.82 cm^2 of a 3 cm^2 emitting surface is made. The collector and guard ring structures include radiation fins coated with Rokide C. The surfaces operate at a temperature less than 750°K.

The leakage current between collector and guard ring is normally 3 to 3 to 4 orders of magnitude below the

0093-3813/78/0600-0191$00.75

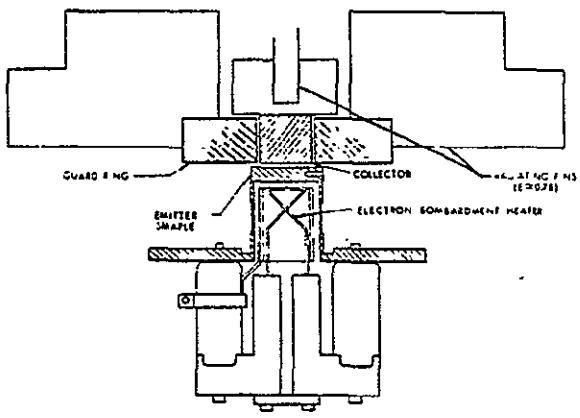

Figure 1. Vacuum emission vehicle components.

current level measured in the collector circuit. The potential of the guard ring is essentially equal to that of the collector under these conditions. Emission measuremets are taken in a vac-ion pumped environment with pressures between 2×10^{-8} and 4×10^{-9} torr. Testing is done after all test fixtures, emission vehicle components and vacuum bell jar have been baked out at approximately 200°C.

Measurement Techniques

The electrode materials were cleaned only with ethyl alcohol before they were installed in the vacuum emission vehicle. Electron emission measurements were taken at a number of emitter temperatures for each sample. At each temperature the emission was measured as a function of the applied field. The saturated emission was determined by generating Schottky plots from the Schottky equation,

$$\log J_{RS} = \log J_R + \frac{1.912}{T}\sqrt{E} \qquad (1)$$

J_R is the zero field Richardson current, J_{RS} is the Schottky current and E is the electric field. The plot of Log J_{RS} versus $\sqrt{E}$ can be extrapolated to determine J_R. J_R is then substituted into the Richardson-Dushman equation, Eq. 2, with J_R equal to J_o.

$$J_0 = A\,T^2 \exp[-\phi_E/kT] \qquad (2)$$

where A = 120 Amps/cm^2°K^2

T = emitter temperature (°K)

ϕ_E = effective work function (ev)

With this, the effective work function is calculated. In appendix A, a complete set of Schottky plots for the experiments performed are presented. Experimentally, the zero field emission J_R is determined from an extrapolation from the linear region of a given Schottky plot at a given temperature. The experimental value is then substituted into Eq. 2 and the effective work function (ϕ_E) is calculated. The slope of any given plot can be checked theoretically by use of Eq. 1.

Sample Preparation

The three primary samples, $LaB_{6.01}$, $LaB_{8.5}$, $LaB_{5.9}$, were prepared by cold pressing. The materials was pre-reacted by arc melting the raw components to make a button. The button was then ground into a fine powder and mixed with alcohol as a binder. The mixture was then placed under a high pressure of approximately 50,000 lb/in^2 to form the sample. The button was then sintered at 1875 to 1975°K for three hours in a high vacuum. After sintering, the samples were surface ground to make them flat and true. They were then polished with carborundum paper to produce a smooth surface. The samples tested are somewhat porous, but the density has not yet been measured.

The $LaB_{5.9}$ sample developed a crack along the top of the sample over the hohlraum. This apparently resulted from the hohlraum fabrication and a subsequent thermal cycle, but the crack has not since propagated.

Experimental Results

Three samples, $LaB_{6.01}$, $LaB_{8.5}$ and $LaB_{5.9}$, were tested and the thermionic emission characteristics of each of these samples was determined.

LaB_6 thermionic Emission Characteristics

Table I shows the thermionic emission history of the LaB_6 sample. The Schottky plots from which the data was obtained are given in Appendix A, Figs. A-1 through A-7. The sample was initially heated at 2037°K for 10 hrs. following sintering. Next, the sample was measured in the vacuum emission vehicle. The initial work function of the $LaB_{6.01}$ was approximately 2.9 ev. The sample was initially light purple in color. Subsequent high temperature treatments at 1800°K for 18 hours and 1400°K for 300 hours did not appreciably change the color of the material although there appeared to be a slight increase in work function.

A drastic change in properties were observed after the sample was vented to air and reheated. The color changed from light purple to a sky blue with spots of silver intermixed, and the work function increased to 4 ev. Apparently the sample became oxidized during venting and the subsequent thermionic emission runs at 1400°K were insufficient to remove the oxide layer. When the $LaB_{6.01}$ surface oxidizes the oxygen will combine chemically primarily with the La forming La_2O_3, which is white. The surface will thereby become richer in B, possibly as high as LaB_9, which is dark blue. The intermixing of the blue and white could result in the sky blue/silver appearing surface. In the areas where Ta was in contact with the surface, the color was purple. This would support the oxygen hypothesis since the Ta has a higher oxygen affinity than the La. The interior remained purple.

The initial high work function of 4 ev is thought to result mainly from the high B composition of the surface. Heating the surface at 1400°K gave rise to an intemediate work function of 3.4 ev. The sample color changed to blue green and repeated emission tests demonstrated that the

TABLE I

$LaB_{6.01}$ THERMIONIC EMISSION HISTORY

T (°K)	J_{R1} $(A/cm^2)(10^{-4})$	ϕ_E (eV)	Conditions
1300	10	2.92	Sample color-purple
1300	16.7	2.86	Activation: 10 hr. 2073°K
1400	58	2.95	
1300	6.2	2.97	Additional 18 hr. at 1800°K
1400	44	2.98	Additional 300 hr. at 1400°K
1300	0.0037	4.07	After Vent-1 Color-sky blue with silver
1400	0.008	4.03	After Vent-2 Color-sky blue with silver
1400	1.0	3.44	Color-blue green
1450	3.4	3.42	Color-blue green
1400	1.3	3.41	Stable emission
1350	0.55	3.37	
1300	0.20	3.35	
1250	0.070	3.33	
1200	0.020	3.32	
1400	110	2.87	Heat treat 1785°K for 24 hrs. Color purple; stable emission
1350	45	2.86	
1300	13.5	2.88	
1250	4.0	2.87	
1200	2.2	2.83	

was very stable for tests run at 1450°K and below. The work function values from 1200°K to 1450°K are given in Table I with Schottky plots shown in Appendix A, Fig. A-4. The surface resulting in the 3.4 ev work function was probably a complex oxy-boride containing a lower concentration of B and O than initially.

The high temperature heat treatment at 1785°K for 24 hours returned the material to its initial condition with a purple color and a stable emission. The emission after the final high temperature heat treatment produced a work function lower than had been obtained after the first high temperature heat treatments. The emission approximately doubled at 1400°K. The final condition of the sample appeared to be very stable as repeated runs produced work functions of 2.83 to 2.87 ev as shown in Table I and Fig. 1-5.

$LaB_{8.5}$ Emission Characteristics

The $LaB_{8.5}$ sample was high temperature treated at 1930°K for 24 hours. After making a series of runs, the sample was again heat treated at 1700°K for 48 hours. The experimental runs after both of these heat treatments were very consistent and repeatable. The work function ranged from 3.18 ev at 1200°K to 3.28 ev at 1450°K as shown in Table II and Fig. A-7.

The color of the $LaB_{8.5}$ sample was dark blue at the beginning of testing and the outer edges of the sample still appeared to be dark blue after all the testing was completed. Sample inspection revealed that only the central portion of the surface which faced the collector had changed from dark blue to purple, similar to that of LaB_6. This color change corresponded to the position of the filament which heated the backside of the sample by electron bombardment. Consequently only that portion which was apparently hotter than the outer edges, changed from $LaB_{8.5}$ to the steady state composition near LaB_6. This sample as well as the $LaB_{5.9}$ was not heated between the surface grinding operation and the thermionic measurements to avoid any changes in the surface composition this would produce. Unfortunately, the considerable amount of volatile impurity retained by the sample produced a very heavy black deposit on the collector which partially flaked off during the study.

$LaB_{5.9}$ Emission Tests

The $LaB_{5.9}$ sample was high temperature treated at 1800°K for 20 hours. It was noted that throughout the tests that the two sides of the sample on either side of the hohlraum had quite different apparent temperatures. For example, for a hohlraum temperature of 1380°K, the high temperature side was 1321°K while the low temperature side was 1280°K. The temperature difference corresponded to an apparent fine crack which extended from along the top of the hohlraum on one side to nearly the entire diameter of the sample.

The initial emission measurement of the $LaB_{5.9}$ sample produced work functions over 3 ev. The results are shown in Table III and in Fig. A-7. These values did not correspond well with the previous data for $LaB_{6.01}$ and it was felt that sufficient thermal threament had not been achieved to remove possible grinding contamination. The higher La content should produce a lower work function than for $LaB_{6.01}$. The sample was then high temperature treated at 1884°K for approximately 18 hours, and then at 2000°K for 12 hours. The resulting work function for the $LaB_{5.9}$ was lowered to approximately 2.9 ev as shown in Table III and in Fig. A-8. Further high temperature treatment at the time was not possible due to a power supply malfunction.

The initial color of the sample was a very dark purple. After the final tests were run, the sample color was observed to have lightened slightly with some tinges of the light purple observed in the LaB_6 sample.

DISCUSSION

LaB_6 is the most important compound of the La-B system for thermionic applications. Table IV compares some literature values for thermionic emission characteristics with those of this work. The work function values for references 1, 2 and 3 were converted from Richardson values to effective values with an $A = 120\ A/cm^2{}^\circ K^2$ in order that straight-forward comparisons could be made. T, J_R, and ϕ_E for each of the tests are listed where they were available. The work function is the viable parameter for comparison since it is a slowly varying function of temperature. J_R of course is a strong function of

TABLE II

THERMIONIC EMISSION CHARACTERISTICS OF $LaB_{8.5}$

T(°K)	J_R $(A/cm^2)(10^{-4})$	ϕ_E(ev)	Conditions
1450	9.7	3.28	Sample heat treated at 1933°K for 38 hrs. and at 1703°K for 48 hrs. Color, dark blue with purple central portion facing collector.
1400	4.75	3.25	
1350	2.4	3.20	
1300	0.78	3.20	
1250	0.265	3.19	
1200	0.074	3.18	

TABLE III

THERMIONIC EMISSION CHARACTERISTICS OF $LaB_{5.9}$

T(°K)	J_R $(A/cm^2)(10^{-4})$	ϕ_E(ev)	Conditions
1450	32	3.13	Heat treated at 1800°K for 18 hrs.
1400	17	3.10	
1350	9.4	3.05	
1300	2.6	3.07	
1250	0.95	3.05	
1400	47	2.97	Further heat treated at 2000°K for 12 hrs.
1350	23	2.94	
1300	10	2.92	
1250	3.4	2.91	
1200	1.35	2.88	

TABLE IV

THERMIONIC EMISSION CHARACTERISTIC COMPARISONS FOR La-B COMPOUNDS

Contributor	Compound	T(°K)	J_R $(A/cm^2)(10^{-4})$	ϕ_E(effective, eV)
Ahmed & Broers[1]	LaB_6	1800	3.24×10^5	2.53
Gallagher[2]	LaB_6	1500-1700		2.80
Lafferty[3]	LaB_6	1400	153	2.83
	LaB_6	1948	3.0×10^5	2.90
Swanson, et.al.[4]	LaB_6(110)*	1600	3.2×10^3	$2.85 \pm .05$
	LaB_6(111)*	1600	2.2×10^3	$2.90 \pm .05$
	LaB_6(100)*	1600	3.5×10^4	$2.52 \pm .05$
	LaB_6(100)**	1600	1.0×10^4	$2.70 \pm .05$
Kudintseva[5], et.al.	$LaB_{5.9}$	1773	2×10^5	2.56
	$LaB_{6.0}$	1773	4×10^4	2.80
	$LaB_{8.5}$	1773	1.8×10^4	2.92
This Work	$LaB_{5.9}$	1400	46	$< 2.97 \pm 0.05$ 11%
	$LaB_{6.01}$	1400	110	2.87 ± 0.05
	$LaB_{8.5}$	1400	4.7	$< 3.25 \pm 0.05$ 16%

* Zone melted

**All flux growth

temperature and since data at the same temperature from all the references were not available, the ϕ_E values are compared.

The LaB_6 work functions reported by Lafferty [2], and Gallagher [3], Kudintseva [5], and by Swanson [4] and for (110) and (111) crystal faces, are within experimental error of that reported in this work for $LaB_{6.01}$. These values are in the range 2.8 to 2.9 ev. The values for LaB_6 reported by Ahmed and Broers [1] is on the order of 2.5 ev. Work functions for the other two compositions recorded in this work, $LaB_{5.9}$, and $LaB_{8.5}$ have also been reported by Kudintseva [5]. The work functions reported in this work are higher in both cases: for $LaB_{8.5}$ there is a difference of 11% and for $LaB_{5.9}$, a difference of 16%.

There are a number of factors which could lead to differences in reported values of work function for a given composition. The emission, and therefore work function, and strong functions of surface composition, emitter temperature, purity ans sample density [5]. The emission and work function are primarily functions of the surface parameters of a material, therefore, the composition of the surface of the sample is certainly a prime determinant in the work function [6].

The attainment of an equilibrium surface composition depends upon the initial sample composition and the time and temperature at which a sample is heat treated. It was seen clearly, for example, in the case of $LaB_{5.9}$ that the heat treating conditions changed the emission and work function quite drastically although this change was probably due to surface impurity removal. The initial surface composition was not known.

Kudintseva's [5] results indicate that the work function rises as the boron content increases. This would be expected since the work function of La is lower than that of B. At a sufficiently high temperature the surface composition will be near the congruently vaporizing composition regardless of the bulk composition. At lower temperatures, (emission measurements here are regarded as low temperature) the surface composition will be more strongly related to the bulk composition [6]. Thus, one would expect to obtain a work function for $LaB_{5.9}$ which is somewhat lower than that for $LaB_{6.1}$. In the work presented here the work function of $LaB_{5.9}$ is slightly higher than that for $LaB_{6.01}$. Again referring to Table III, it might be argued that were further heat treating available for this sample or were a higher temperature attained, the surface composition may have shifted nearer to that of the congruent vaporizing composition, $LaB_{6.01}$ so that the work function would have been equal to or lower than that for $LaB_{6.01}$.

The work function for $LaB_{8.5}$ presented in this work is also higher that that reported by Kudintseva. However, the lack of uniformity in surface color suggests that further heating will produce a lower work function.

Another important parameter is purity. A case at hand is the apparent contamination of the $LaB_{6.01}$ sample with oxygen during venting. As seen in Table I, the work function rose by approximately 40% to over 4 ev after venting and then returned to the initial value after heat treatment. Gross contamination by surface grinding appeared to dominate results obtained from the $LaB_{5.9}$ sample, and to a lesser degree the $LaB_{8.5}$ sample during the initial measurements.

The samples examined in this work were approximately 1.9 cm in diameter. The collector and guard ring were approximately 15 cm in diameter. The large sampling area resulted in currents which surpassed the limits of the measuring circuit. The result was that Schottky plots were limited to approximately 1400°K and outgassing was limited to a maximum of 2000°K. A new system is being built which will accommodate samples which are approximately 20% the cross sectional area of those used here. Outgassing and maximum emitter temperature limitations will thus be avoided in the future.

CONCLUSIONS

Relatively good agreement was obtained for work function values between this work with a composition of $LaB_{6.01}$ and measurements of a number of other workers for compositions nominally LaB_6. A number of factors might be involved in the differences that were noted, including sample fabrication and specifically sample density, surface composition, purity, grain structure (preferred orientation), and possible measurement differences. These and other factors need to be clearly accountable so that consistency in data comparisons can be obtained.

The apparent oxide surface produced on the $LaB_{6.01}$ is an example of the large variation in thermionic emission properties that can result from surface contanination.

The effect of processing is seen to be an important factor as demonstrated by the heavy depositis from the $LaB_{8.5}$ and $LaB_{5.9}$.

The relationship between emission properties and bulk composition have been demonstrated through these tests, with the obvious result that extensive measurements are yet required to establish exact relationships between emission properties, temperature, surface and bulk composition, and evaporation properties. An understanding of these characteristics should lead to the development of compounds with greater long term stability coupled with enhanced emission properties leading to more efficient thermionic converters.

ACKNOWLEDGEMENTS

The assistance of Mr. Tom Kouts and Jim Jaskie in the laboratory is gratefully acknowledged.

Support of this work by NASA Lewis Research Center is deeply appreciated.

REFERENCES

1. Ahmed and Broers, *J. Appl. Phys.*, **43**, 5, 2185 (1972).
2. J. M. Lafferty, *J. Appl. Phys.*, **22**, 299 (1951).
3. H. E. Gallapher, *J. Appl. Phys.*, **40**, 1, 44 (1969).
4. L. W. Swanson and D. R. McNeely, Work Electrotechnical Congress, Moscow, to be presented, (June 21-25,

1977).
5. G. A. Kudintseva, G. M. Kuznetsova, F. G. Mamedov, G. A. Meerson, and B. M. Tsarez, Izvestiya Akademmi, Nauk, SSSR Neoganicheskie Materialy, 4, 1, 49-53 (January 1968).
6. E. K. Storms, and B. Mueller, to be published, Journal Of Physical Chemixtry, (1977).

APPENDIX A

Schottky Plotts for LaB_6, $LaB_{8.5}$, $LaB_{5.9}$

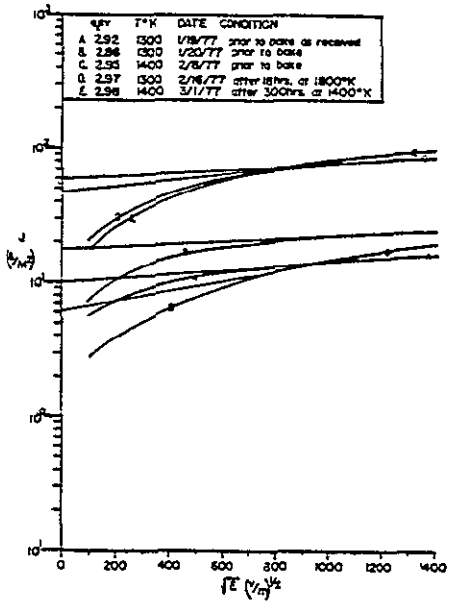

igure A-1. $LaB_{6.01}$ emission history prior to venting.

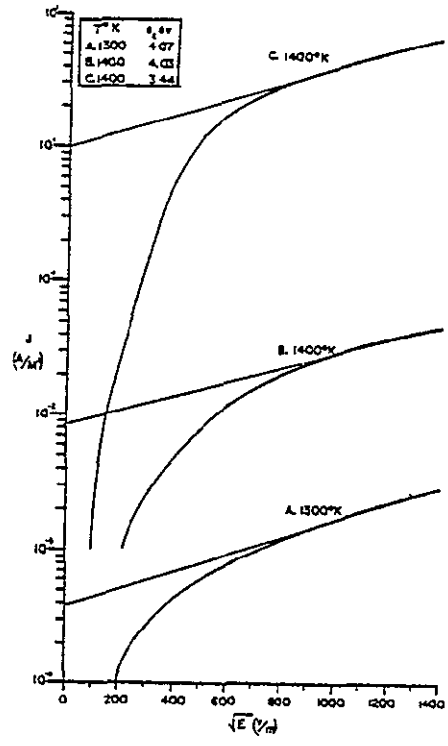

Figure A-2. $LaB_{6.01}$ following venting. A-B Sky Blue/ Silver, C. Blue-green surface color.

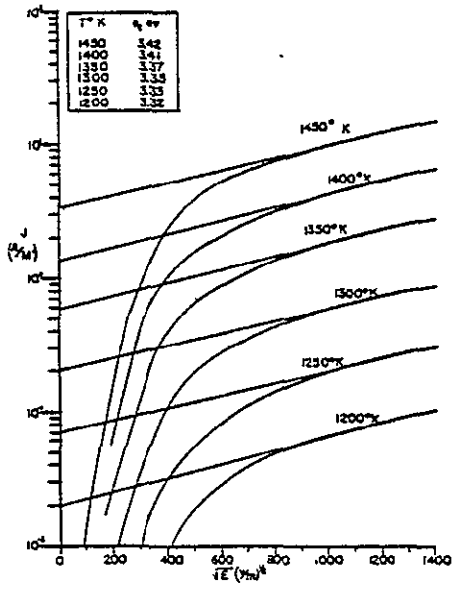

Figure A-3 $LaB_{6.01}$ stable emission from blue-green sample.

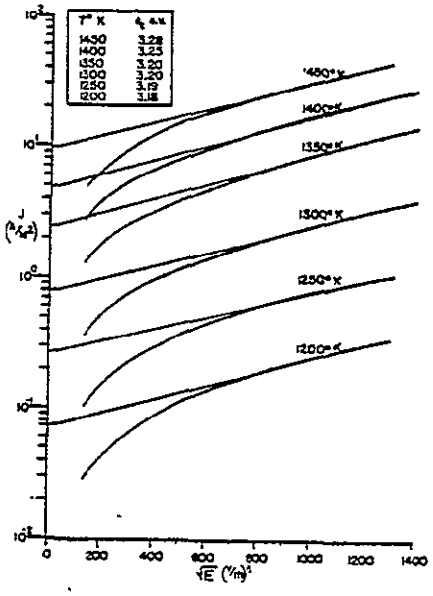

Figure A-5 $LaB_{8.5}$ sample emission.

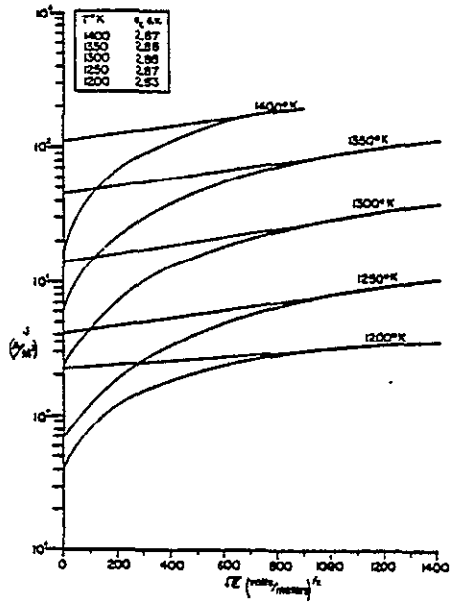

Figure A-4 $LaB_{6.01}$ stable emission after 24 hours at 1875° K. Purple color

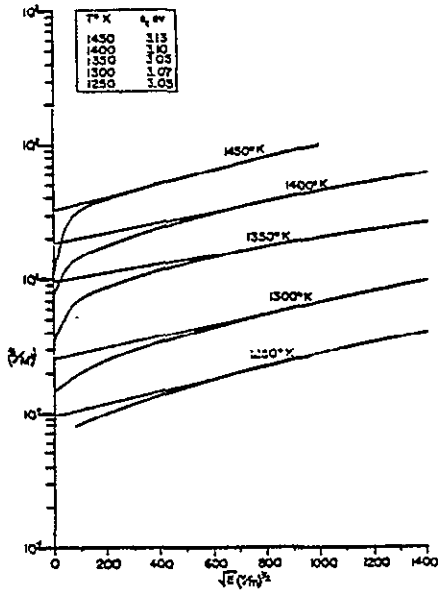

Figure A-6 $LaB_{5.9}$ stable emission following 20 hours at 1800° K.

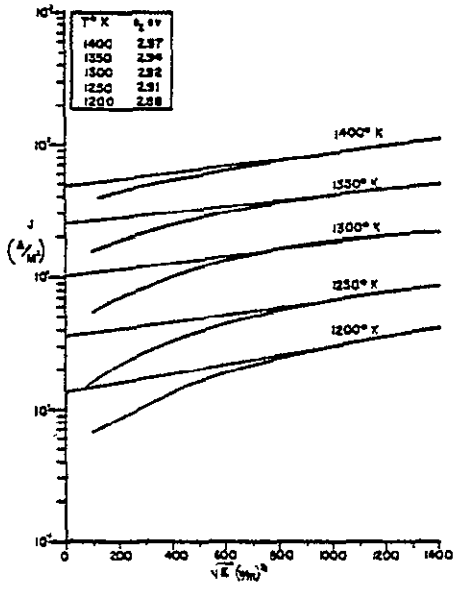

Figure A-7 $LaB_{5.9}$ stable emission following 20 hours at 2000° K.

The first sample similar to those in Fig. 11 was niobium carbide sample containing .98 to .99 percent carbon. It was hot pressed at 2773°K in a graphite die at 6.9 MN/m^2. The sample was subsequently ground flat and outgased in a vacuum at about 1773°K. The holder shown for the sample consists of a molybdenum base plate, a tantalum heat choke and a tantalum base plate just underneath the sample disk. The tantalum base plate will be heated by electron bombardment and the sample will then be heated by radiation coupling to the tantalum. This sample holder was used specifically so that sample disks could be used interchangeably with the same sample holder. The sample holder fits both of the existing vacuum emission systems and also the thermionic emission microscope. Both vacuum emission measurements and thermionic emission measurements in the thermionic emission microscope will be used to determine the work function and surface characteristics of these samples.

The complete results from the work function measurement study of Lanthanum-Boron Compounds is presented in the publication attached. Thus, this paper is inserted here for completness. It should be noted that the Abstract was incorrect. Apparently an abstract by Dr. E.K. Storms for another paper was inadvertently substituted for the original one when the paper was being processed at LASL.

The three samples shown in Fig. 11 are lanthanum-boron samples.

6) Measurement of Gaseous Emission Properities Using a Marchuk Tube

The electron emission properities of candidate thermionic electrode materials was investigated in a typical Marchuk experiment.

A glass test vehicle was designed for these tests. Candidate emitter materials were used as Langmuir probes in a plasma generated by secondary electrodes.

The Marchuk technique involves a plasma immersion process whereby materials of interest are allowed to emit thermionically into a surrounding plasma. Work functions may thus be measured at various plasma-gas pressures. Typically, wire probes have been utilized, their temperatures being determined by pyrometry at elevated temperatures, and by temperature-resistivity correlations at low temperatures.

The complete evaluation of cesiated measurements of Nickel, Inconel 600 and Haslelloy X are presented in the literature. This section is thus the same as the IEEE publication which is inserted and also is attached at the end.

7) Summary of Results

The vacuum emission devices was operational, although the high vapor pressures of some super alloy elements and low emission current densities at low emitter temperatures, 1200°K - 1400°K, have indicated that further refinements be made. These have included the acquisition of a metal bell jar in order to produce high vacuums, 1.3×10^{-7} N/m^2, with an all metal gasketed system. Some of the super alloys appeared to be unsatisfactory for thermionic electrodes because of high vapor emission characteristics of some elements such as manganese. Mass spectroemter evaluations of some high temperature super alloys confirmed the very high vaporization results; as more super alloys are evaluated, the vaporization trends of the various elements will be determined. From these studies it might be possible to choose or design super alloys of particular compositions which might be suitable for thermionic electrodes.

High temperature physical properties including tensile strength, yield strength, stress to rupture, and creep strength have been obtained from the literature for a number of candidate super alloys. The high

temperature corrosion behavior of some of these alloys and also of a couple of stainless steels have been obtained from the literature. An important application for low temperature, low cost thermionics is as topping a device for conventional steam power plants. It is probable that sodium could be used as a heat transfer medium from the combusting gases to the thermionic element. Super alloys might be used both as a thermionic electrode and also as the plumbing for the sodium heat transfer lines. A good deal of information exists in the literature in regard to compatibility of various stainless steels with sodium. Most of the experimental work that is in the literature was produced for the liquid metal fast breeder reactor program. The same corrosion considerations would be necessary in utilizing sodium in thermionic topping, as would be required for the LFMBR programs. Little information currently exists in the literature in regard to the alkali metal compatibility with super alloys. The LFMBR programs are now beginning to examine alkali metal - super alloy compatibilities because the strength of the candidate stainless steels are not sufficient for some projected LFMBR applications. It is very probable that this information could become important to thermionics should such materials be used for thermionic topping. At the present the most important corrosion parameters appear to be the oxygen content of the sodium and the flow rate. The mechanical properties of super alloys must also be evaluated in the sodium atmosphere. At the present little information is available with regard to the behavior of super alloys with alkali metals in general.

One niobium carbide sample has been fabricated by Los Alamos Scientific Laboratories and is now being instrumented for vacuum emission tests at Arizona State University. After preliminary testing is done with this

first sample, a series of closely controlled carbide alloys will be prepared by Los Alamos and tested in the mass spectrometer both before and after vacuum emission tests are made for work function determination. The results of these tests will be evaluated in order to try and determine the bonding characteristics of such alloys. If this is understood, it should be possible to tailor the work function of a given thermionic emitter hopefully to a given desired value. The series of other metals including zirconium with carbon, with boron, and possible borocarbides or boronitrides are intended for investigation during this program.

Plans are underway for the fabrication of the Marchuk tube in order that cesiated emission from the carbide samples and possibly some super alloys can be performed at ASU. These systems have been used successfully in the past and are fairly simple to evaluate, and hopefully can provide a good deal of information.

Relatively good agreement was obtained for work function values between this work with a composition of $LaB_{6.01}$ and measurements of a number of other workers for compositions nominally LaB_6. A number of factors might be involved in the differences that were noted, including sample fabrication and specifically sample density, surface composition, purity, grain structure (preferred orientation), and possible measurement differences. These and other factors need to be clearly accountable so that consistency in data comparisons can be obtained.

The apparent oxide surface produced on the $LaB_{6.01}$ is an example of the large variation in thermionic emission properties that can result from surface contaminination.

The effect of processing is seen to be an important factor as demonstrated by the heavy deposits from the $LaB_{8.5}$ and $LaB_{5.9}$.

The relationship between emission properties and bulk composition have been demonstrated through these tests, with the obvious result that extensive measurements are yet required to establish exact relationships between emission properties, temperature, surface and bulk composition, and evaporation properties. An understanding of these characteristics should lead to the development of compounds with greater long term stability coupled with enhanced emission properties leading to more efficient thermionic converters.

The electron emission characteristics were measured for nickel, Inconel 600, and Hastelloy X probes with a 412 K cesium reservoir. The nickel alloys were shown to have peak electron emission 1.4 to 2.1 times greater than pure nickel. Both the Inconel and the Hastelloy samples had work functions of 1.64 eV at peak emission. The minimum cesiated work functions were estimated to be 1.37 eV at a probe temperature of 750 K for Inconel and 1.40 eV for Hastelloy at a probe temperature of 665 K. ϕ_0 for both alloys is estimated to be approximately the same as pure nickel, 4.8 eV.

BIBLIOGRAPHY

1. Materials Data Handbook: Inconel Alloy 718, R.F. Muraca, et al (Western Applied Research and Development, Inc.) April, 1972.

2. Military Handbook-5A, Dept. of Defense, "Metallic Materials and Elements for Flight Vehicle Structures," FSC 1500, February, 1966; latest change order January 1970.

3. International Nickel Co., Huntington Div., "Inconel Alloy 718," February 1968.

4. Rocketdyne/North American Rockwell, MFS-18388 in "Metallury: A Compilation," NASA SP-5940 (01), 1970.

5. International Nickel Company, Huntington Div., Basic Data Report, "Inconel 718, Age-Hardenable Nickel-Chromium Alloy," September 1960.

6. The Effect of High Temperature Sodium on Mechanical Properties of Candidate Alloys for the LMFBR Program - Contract AT (11-1) - 765, May, 1968, Andrews and Barker, Authors. MSA Research Corporation, Evans City, Pennsylvania.

7. Mechanism of Fe and Cr Transprot by Liquid Sodium in Non-Isothermal Loop Systems, - by B.H. Kolster, Metaalinstituut TNO, Apeldoorn, The Netherlands August 30, 1974.

8. Corrosion in Polythermal Loop Systems
II. A solid-State Diffusion Mechanism With and Without Liquid Film Effects by R.B. Evans, III, J.W. Koger and J.H. DeVan, Oakridge National Lab, June, 1971.

9. The Corrosion and Mass Transfer of Pure Iron, Nickel, Chromium and Cobalt in 660°-760° C Sodium - by A.H. Fleitman and H.F. Isaacs - Brookhaven National Laboratory - Upton, New York.

10. A Statistical Analysis of Hot Corrosion Tests of Some Experimental and Commerical Super Alloys - R. Field, D.J. Fisk, and H. Von E. Doering, Materials Laboratory Laboratory Naval Ship Research and Development Center, Washington, D.C.

11. Mäss Transfer Effects in Some Refractory-Metal-Alkali-Metal-Stainless Steel Systems by J.R. diStefano, November, 1966, Oakridge National Laboratory.

12. Affect of High Temperature Sodium on the Mechanical Properties of Candidate Alloys for the LMFBR Program - May, 1967 - MSA Research Corporation, sponsored by US Atomic Energy Commission, Chicago Operations Office, Oregon, Illinois, by R.C. Andrews and K.R. Barker.

13. What are the Effects of Alloying Elements Singly or in Combination on Hot Corrosion - by A. Davin and D. Coutsouradis, Centered Derecharches Metallurgiques, Belgium.

14. Are Cobalt Based Alloys Intrinsically More Resistant to Hot Corrosion Than Alloys Based on Nickel by W.L. Wheatfall, Naval Ship Research and Development Center, Annapolis, Maryland, U.S.A.

15. Corrosion of Type 316 Stainless Steel With Surface Heat Flux 1200°F Flowing Sodium - by J. Hopenfield, Atomics International North American Rockwell.

16. Process Environment Effects on Heat Pipes for Fluid-Bed Gasification of Coal by D.C. Strimbeck, D.C. Sherren and E.S. Keddy, The 9th Inter-Society Energy Conversion Engineering Conference, San Francisco, California, August 26-30, 1974.

17. Fabrication of Hastelloy Alloys, Technical Bulletin, Sattelite Division of Cabot Inc., 1974.

18. The Application of Directional Solidification to a NASA Nickel-Base Alloy (TAZ-8B), J.C. Freche, W.J. Waters, and R.L. Ashbrook, SAE Mid-Year Meeting, May 1968.

19. Compatibility of Liquid and Vapor Alkali Metals With Construction Materials by J.H. Stang, E.M. Simons, J.A. DeMastry and J.M. Genco Defense Metal Information Center, Battelle Memorial Institute, Columbis, Ohio 43201.

IEEE Transactions on Plasma Science, Vol. PS-6, No. 2 June 1978

ELECTRON EMISSION FROM NICKEL AND ALLOY SURFACES IN CESIUM VAPOR

M. Manda* (Student) and D. Jacobson (Associate Professor)
Arizona State University
School of Engineering
Mechanical Engineering Department
Tempe, Arizona 85281
Received July 19, 1977

ABSTRACT

The cesiated electron emission was measured for three candidate electrodes for use as collectors in thermionic converters. Nickel, Inconel† 600 and Hastelloy+ were tested with a 412°K cesium reservoir. Peak emission from the alloys was found to be comparable to that from pure nickel. Both the Inconel and the Hastelloy samples had work functions of 1.64 ev at peak emission. The minimum work functions were estimated to be 1.37 ev at a probe temperature of 750°K for Inconel and 1.40 ev for Hastelloy at 665°K. The bare work function for both alloys is estimated to be approximately the same as for pure nickel, 4.8 ev.

INTRODUCTION

The thermionic emission properties of nickel and two nickel alloys were investigated using the plasma-anode technique developed by Marchuk [1]. This technique has been used by Houston [2, 3] and others [4, 5] to measure the full temperature range electron emission of both refractory and nonrefractory metals in cesium vapor.

The plasma-anode method utilizes the plasma of a cesium vapor discharge tube to collect thermionically emitted electrons of wire. The probe is completely immersed in the plasma and is run a few volts negative with respect to probe floating potential such that only ions reach the probe from the plasma. Cesium ions thus create a small ion current to the probe, permitting a much larger election current to be emitted without encountering a negative space-charge barrier. This precludes making zero-field measurements. However, Houston and Webster [3] have shown that the expected conventional Schottky effect is not a large source of error in plasma-anode measurements. Further problems arise due to the inability to specify the probe temperature with high precision.

The purpose of this work was to measure the thermionic emission from two nickel alloys which could be used as emitters in thermionic converters. It was intended that common materials possessing adequate high temperature properties (e.g., creep strength, corrosion resistance) be chosen to ultimately reduce the cost of thermionic converters. The alloys chosen for analysis were nickel based super alloys, Inconel 600 and Hastelloy X.

Due to the alloy nature of the test materials, the probes were not heated above 1400°K during both vacuum processing and experimental measurements. It was intended that this treatment promote the formation of stabel high temperature alloys whose surface compositions and hence properties remained constant.

All of the measurements reported were performed at one cesium pressure. The choice of reservoir temperature (T_r) was orbitrary but was chosen to be 412°K to facilitate comparison of results with existing data. Below 373°K, stable plasma arcs at moderate voltages were difficult to obtain. Above 473°K, the glass discharge tube would discolor due to reaction with the cesium vapor.

EXPERIMENTAL APPARATUS

The experimental tube, shown in Fig. 1 was fabricated from Corning type 7052 glass. The press leads, on which the probes are mounted, utilized uranium glass transitions and .102 cm diameter tungsten lead-throughs. A four-lead press was used to support and conduct current to a counterwound spiral cathode of .051 cm tungsten wire. The anode was a 2.54 cm tantalum disk on a two-lead press.

The probes were constructed as shown in Fig. 2. The nickel (99.97% Ni) and the Inconel 600 (73.7% Ni, 16% Cr, 8.4% Fe, 0.35% Mn, balance Cu, Si, C, S) were nominally 0.254 cm in diameter, while the Hastelloy X (48.22% Ni, 20.87% Cr, 17.87% Fe, 9.02% Mo, 2.10% Co, balance Mn, Si, W, Al) was 0.386 cm in diameter. These probe wires passed through double-holed alumina insulators and formed small loops about 1 cm in diameter at one end. The length of each of the exposed loops was determined from photographic enlargements of the probe tips, and each was found to be about 3.1 cm long. The length and diameter of the probe loops were known, and the emitting areas were thus calculated. A summary of the probe characteristics is given in Table I. The ends of each probe were sopt welded directly on two of the press leads. The third press lead was attached to a length of tantalum rod. This was used to simultaneously support the probe-insulator assembly and serve as the guard ring current lead. After each probe was assembled all exposed metal areas except the probe tip were painted with high purity alumina powder in distilled water to minimize possible electron discharge from these areas. The probe assemblies were connected to the main tube body with side tubes, the inside of which were painted with

* Currently an engineer with Rasor Associates.
† Registered trademark of the International Nickel Co., Inc.
+ Registered trademark of the Cabot Corporation.

0093-3813/78/0600-0200$00.75

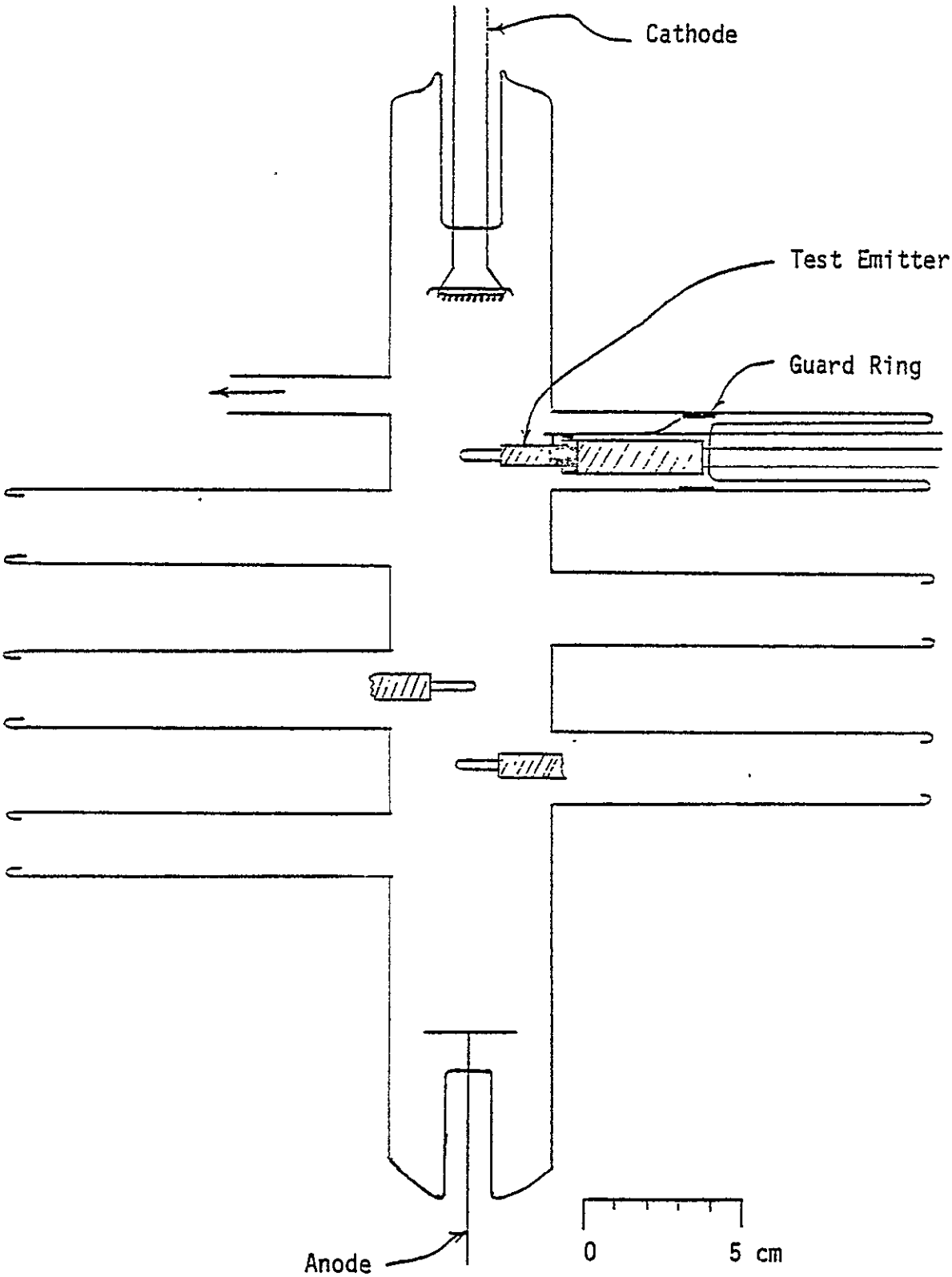

Figure 1. Experimental Tube

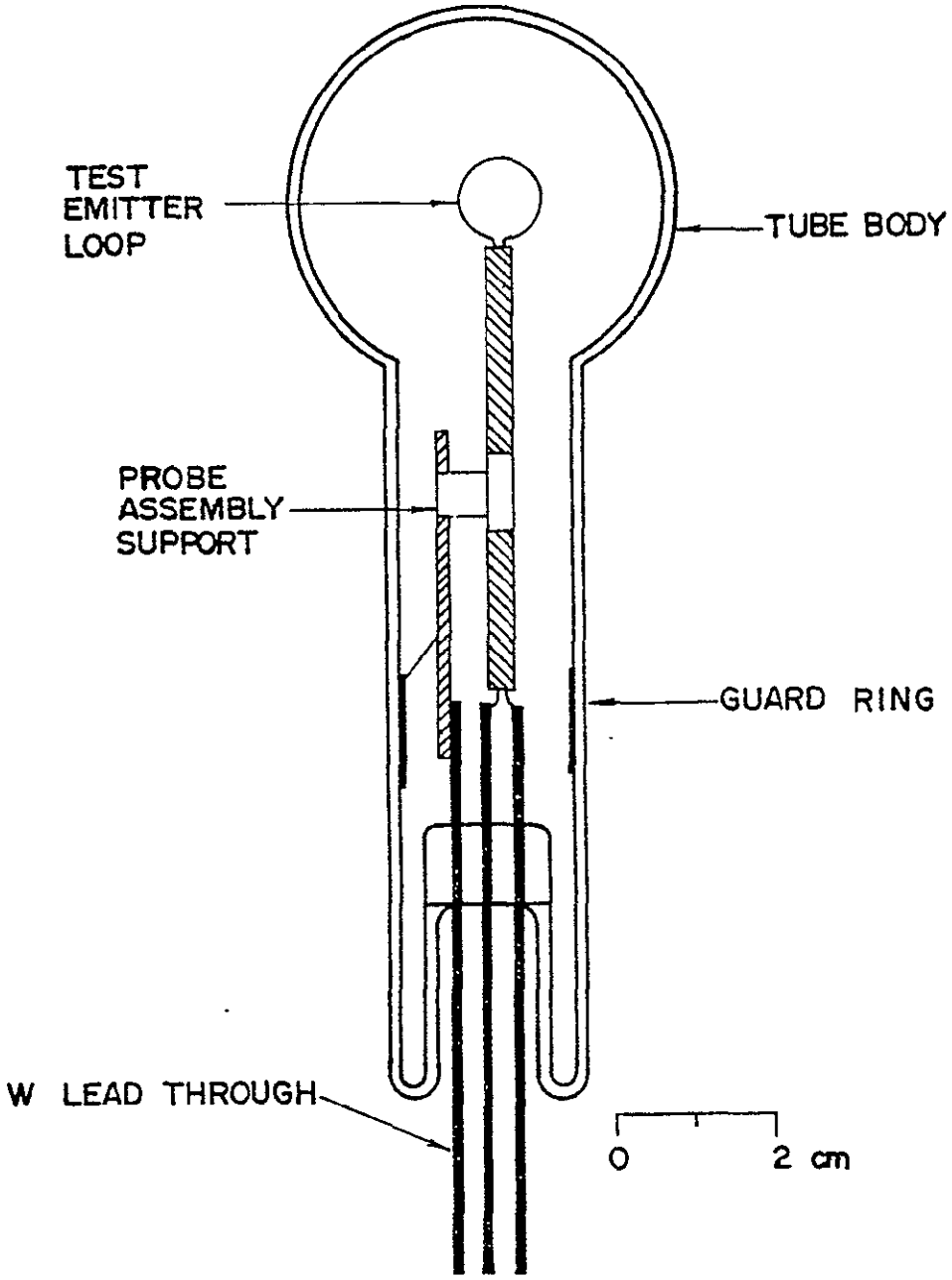

Figure 2. Probe Detail

tantalum spring wiper was used to contact the guard ring and was connected to the guard ring press lead with a 0.254 cm nickel wire.

The assembled tube was evacuated and baked out at 530°K for one week. The pressure in the hot tube was 3×10^{-7} torr before seal-off. The cesium reservoir, connected remotely to the main tube, was baked out to 460°K. The cesium ampoule was broken just prior to seal-off, by dropping a magnetic breaker rod onto a scribed portion of the cesium ampoule. A slight pressure rise was noted when the ampoule broke, but the pressure quickly returned to 3×10^{-7} torr. The tungsten cathode was outgassed at 2500°K for three hours and each probe was outgassed at 1350°K for 30 minutes.

A micro-optical pyrometer was used to measure probe temperatures above 1200°K. Measurements, however, were rendered difficult by cathode reflections from the probe. Nonetheless, suitable measurement areas were found on probe surfaces which faced away from the cathode. Below 1120°K, temperatures were specified by extrapolation of pyrometer temperatures correlated to the peak-to-peak ac power supplied to each probe. Probe temperatures are believed to be accurate to within ±30°K or better. This, in general, produces an uncertainty of ± 0.1 ev in work function values calculated for the probes.

To insure probe temperature uniformity, two factors were incorporated in the probe design. First, the length of the exposed loop was made much smaller than the total

TABLE 1.

Probe No.	Material	Wire Diameter (cm)	Exposed Length (cm)	Emitting Area (cm^2)
1	Ni	0.0249	2.927	0.2290
2	Inconel 600	0.0254	3.048	0.2432
3	Hastelloy X	0.0386	3.124	0.3788

wire length. Second, stainless steel bushings were used to center the emerging wires in the channels of the alumina insulators. Pyrometer temperature readings on the hot probes indicated temperature uniformity better than 10°K.

The entire tube was placed in an oven whose door had been modified to permit viewing of the tube. The cesium reservior was outside the oven in a mineral oil bath thermostated to ± 0.25°K. All connecting tubing and the main tube itself were kept at least 15°K above the reservoir temperature to minimize the occurrence of cold spots. During operation, the cesium remained at several scattered spots in the reservoir area, indicating bath temperature uniformity.

MEASUREMENT TECHNIQUES

Figure 3 shows the experimental circuit and defines the variables of interest. All circuitry to the left of the tube relates to the production and maintenance of the main discharge, and all circuitry to the right of the tube relates to probe measurements. Probe current measurements, with the gross emission I_p, were made for steady state conditions. A typical set of probe emission characteristics is shown in Fig. 4. The probe heating current is I_f. With $I_f = 0$ (cold probe) the probe acts like a typical Langmuir probe. For a probe voltage, $V_p < \sim -10$ volts I_p is all ion current from the plasma. Below this value of V_p, the probe collects plasma electrons thus destroying the ion sheath at the surface. As the probe is heated, electrons are emitted and I_p changes, going through a maximum and subsequently decreasing. The current with $I_f = 0$ is I_{po}, and the electron current from the probe is then $I_p - I_{po}$ (for $V_p < -10$ volts). This is defined as I_e. The slight increase in I_p with increasingly negative voltage V_p is due to the anomalous Schottky effect.

The data for the Hastelloy probe was collected at one set of discharge conditions. The nickel and Inconel probes were run also at an additional set of conditions so that the results from the two conditions could be compared. The first discharge parameters were arbitrarily set with the cathode heating current, I_K set at 13.7A, the discharge current I_d at 0.8 A and the discharge voltage at 21 V_d. In this operating regime a slight plasma instability was noticed near the anode. This appeared to have little effect on I_p as viewed on the oscilloscope traces. The second discharge parameters were I_K = 17.8 A, I_d = 3.2 A, $V_d \approx 20$ V. This produced a plasma with no apparent instabilities at the anode. Initially, curves similar to those of Fig. 4 were produced for each probe. V_p was chosen by inspection of the I-V characteristic such that for $I_f = 0$, the ion current was saturated. This generally indicated a V_p of about 5 to 6 volts more negative than the probe floating potential (V_p with $I_p = 0$). Subsequent probe data were taken at this value of V_p, unless other wise noted.

With V_p fixed, I_f was varied to change the probe temperature. Prior to measuring I_p, the probe temperature was allowed to equilibrate for three minutes. The effects of prolonged operation at high temperatures (~ 1300°K) or extended ion sputtering with 40 volt cesium ions was also investigated.

EXPERIMENTAL RESULTS

The results are plotted in the form of Langmuir "S" curves and Rasor-Warner [6] plots. Langmuir "S" curves are plots of electron emission current density, J_e as a function of probe temperature, T_p. Theoretical values of work function calculated from the Richardson-Dushman equation with A = 120 $cm^2°K^2$ are shown in the plot also. The Rasor-Warner plots are of the cesiated work function, ϕ against the ratio of probe to cesium reservoir temperature, T_p/T_r. Overlying theoretical curves are for the corresponding bare work function from the Richardson-Dushman equation. The effective surface work functions were also calculated with the Richardson-Dushman equation with A = 120 $A/cm^2°K^2$.

The emission characteristics for the probes are shown in Figs. 5 - 7. Plots of J_e, versus $10^4/T_p$ produces typical "s" curves. For all the probes, peak emission was initially low. This phenomenon was encountered by Houston [2] and Wilson [7] in their investigations of nickel emission in cesium, and thus might be expected for alloys containing nickel.

After the initial measurements, the Ni probe was flashed to 1400°K for one hour 20 minutes to clean the surface. The peak emission increased from 0.041 A/cm^2 to 0.13 A/cm^2 at T_p = 948°K and a T_r = 412°K as shown in Fig. 5. This is in agreement with literatures values [2]. This emission increase, however, was transient; electron current density dropped to near the initial value after 30 minutes. This behavior was evident after subsequent flashings of the probe, as well as after bombardment with 100 volt cesium ions. Contamination of the tube atmosphere is suspected to be the cause, perhaps being confirmed by the unusual shape of the electron emission "S" curve (Fig 5) for $T_p < 948$°K. The emission in this region is

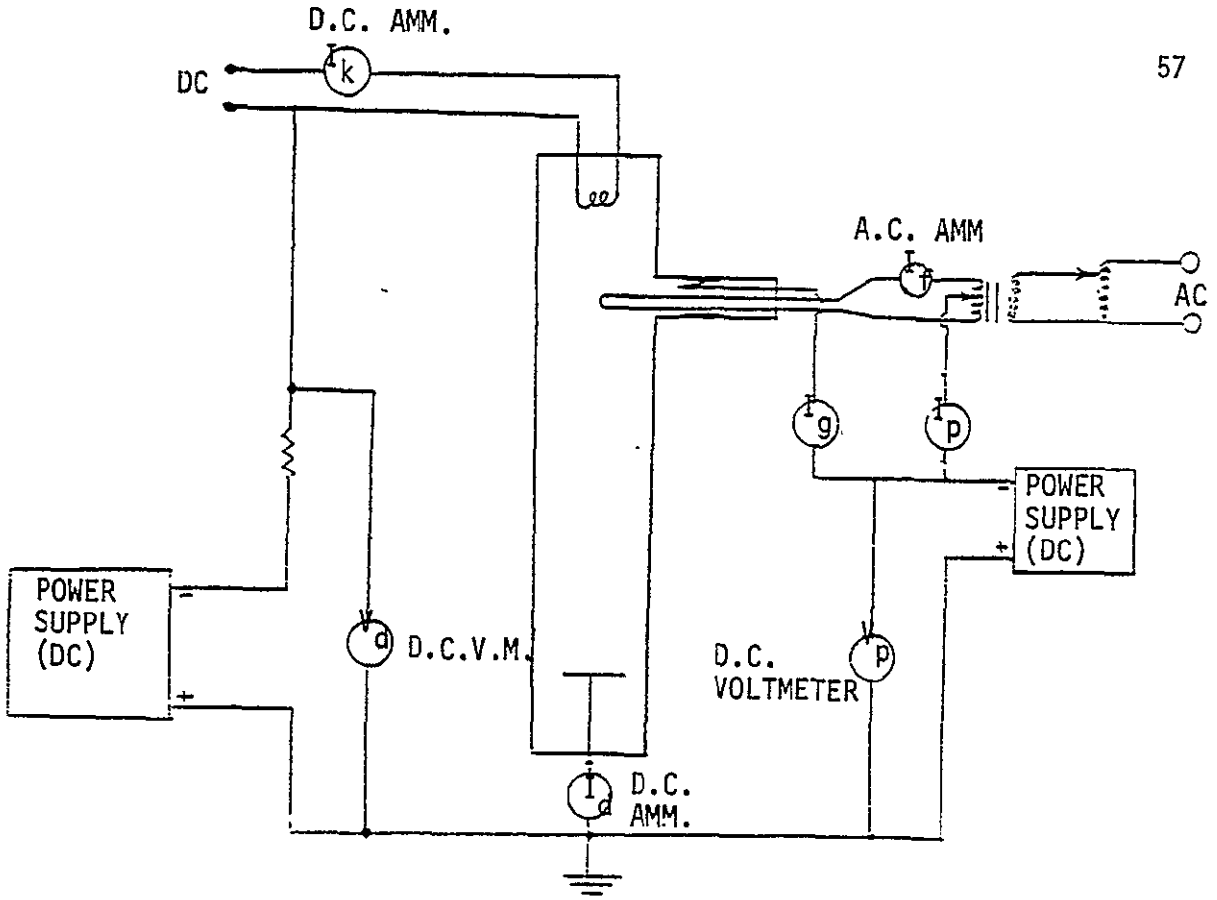

Figure 3. Experimental Circuit Schematic

higher than might be expected, perhaps due to the presence of an adsorbable gas in the tube. No further testing of the Ni probe was undertaken. Its main purpose was to confirm proper operation of the Marchuk tube.

Similar procedures were followed with other probes. After flashing the Inconel probe to 1385°K for 10 minutes, the emission was measured in one minute intervals rather than the normal three minute intervals. Peak emission increased from 0.12 A/cm^2 to 0.26 A/cm^2 at T_p = 943°K and T_r = 412°K as shown in Fig. 6. This emission decreased slowly, but remained in the 0.20 A/cm^2 range. To investigate the effect of prolonged operation at high temperatures, the probe was reheated to 1385°K and run for 2.5 hours. Emission measurements were taken after this period and found to be consistently lower than the 0.26 A/cm^2 value measured after only 10 minute operation at high temperature. The final result in Fig. 6 show peak emission of .18 A/cm^2 at T_p - 943°K with $\phi \approx 1.64$ ev. Although no plateau exists because of temperature limitations, the bare work function can be estimated from the Rasor-Warner plot. The position of the experimental plot can be estimated to $\phi_o \approx 4.8$ ev.

Figure 7 shows the Rasor-Warner plot for the Inconel. Estimations from Figs. 6 and 7 yield a minimum of ϕ of approximately 1.35 ev at T_p = 714eK.

The Hastelloy X probe behaved similar to the Inconel as shown in Fig. 8. After flashing to 1400°K for 45 minutes the emission increased from 0.14 A/cm^2 to 0.18 A/cm^2 at T_p = 939°K. An attempt was made to run this probe at a high temperature for an extended period of time, however, about after 5 minutes the spot welds connecting the probe to the press leads opened. This, of course rendered the probe inoperable for the remainder of the experiment. The "S" curves in Fig. 8 are, nonetheless, essentially representative of the true electron emission from Hatelloy X. $\phi \approx 1.64$ ev for the emission peak.

A Rasor-Warner plot for Hastelloy X is shown in Fig. 9. From Figs. 8 and 9 is $\phi \approx 1.40$ at T_p = 665°K. It is also of note that the plot shows a plateau at ϕ = 2.82 ev. An anomaly exists in that the position of the experimental curve coincides with the theoretical curve for $\phi \approx 4.8$ ev although a plateau is seen at 2.82 ev. The plateau does not follow that expected for a material with $\phi_o \approx 4.8$ ev, but it has been shown by other workers that Ni[7] and some Ni[2] based alloys can display a double minimum in emission due to impurities which might lead to a false interpretation of ϕ_o.

CONCLUSIONS

The nickel alloys were shown to have peak electron emissions 1.4 to 2.1 times greater than pure Ni. In addition, both alloys were estimated to have $\phi \approx 4.8$ ev, the same as that for pure Ni[7]. These alloys, then appear to be

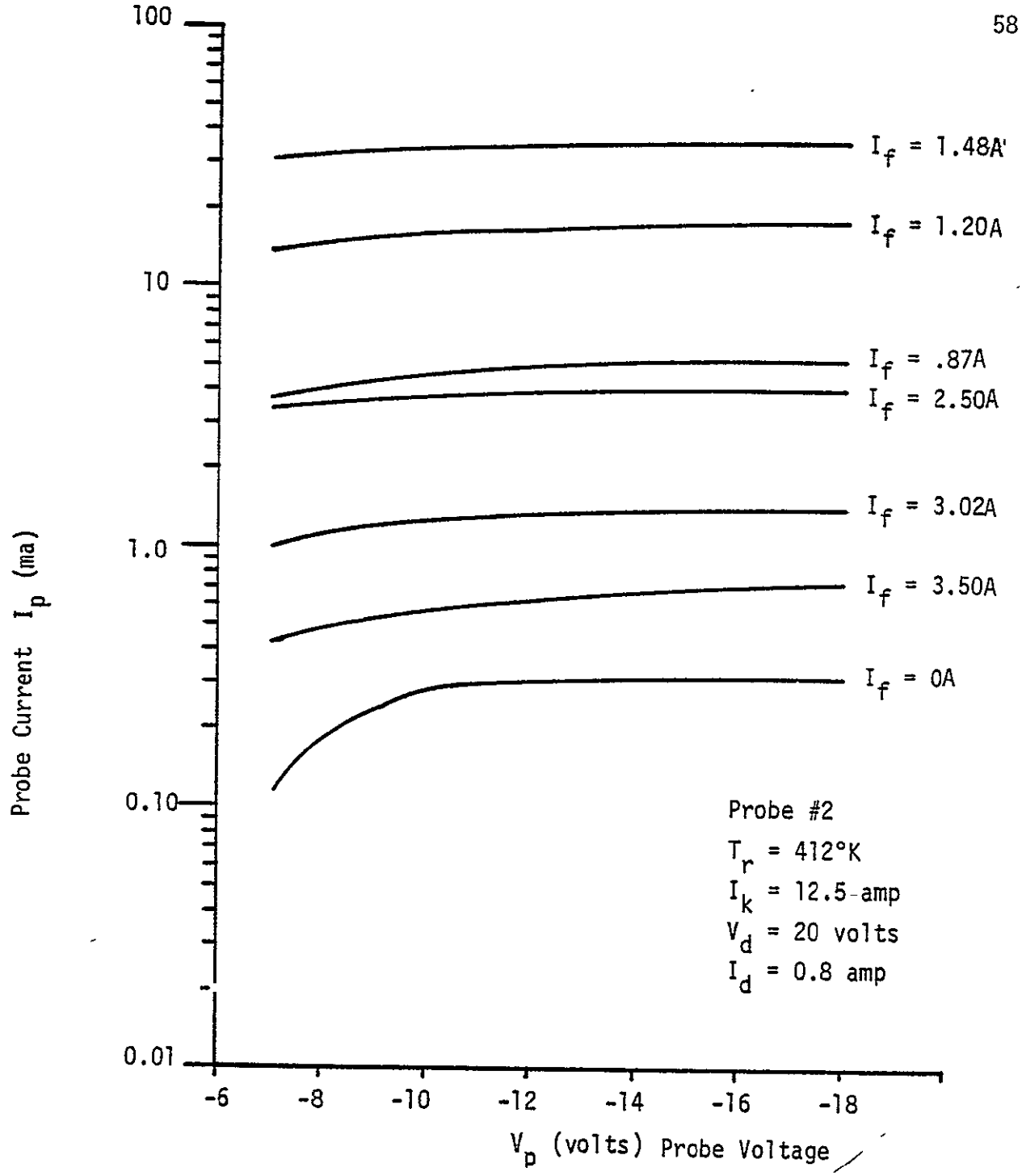

Figure 4. Typical Probe Current Characteristics (Inconel 600)

promising electrode materials for low temperature thermionic devices. Nonetheless, some problems are apparent. Primarily, it was observed that even at moderate temperatures (1100°K) small amounts of material were evaporated from the surfaces. Quantitative evaporation studies have been made on superalloy Incoloy 800 which predict the loss rates of the constituent elements [8]. Atom evaporation studies along with electron emission measurements will be necessary for selection of high effeciency long life thermionic converters. The effects of contamination must be investigated to minimize errors associated with the presence of desirable or undesirable adsorbable gases in the tube.

ACKNOWLEDGEMENTS

This work was carried out under NASA Grant NSG 7019 through NASA Lewis Research Center. The authors also gratefully acknowledge contributions by M. Wheeler and G. Fitzpatrik.

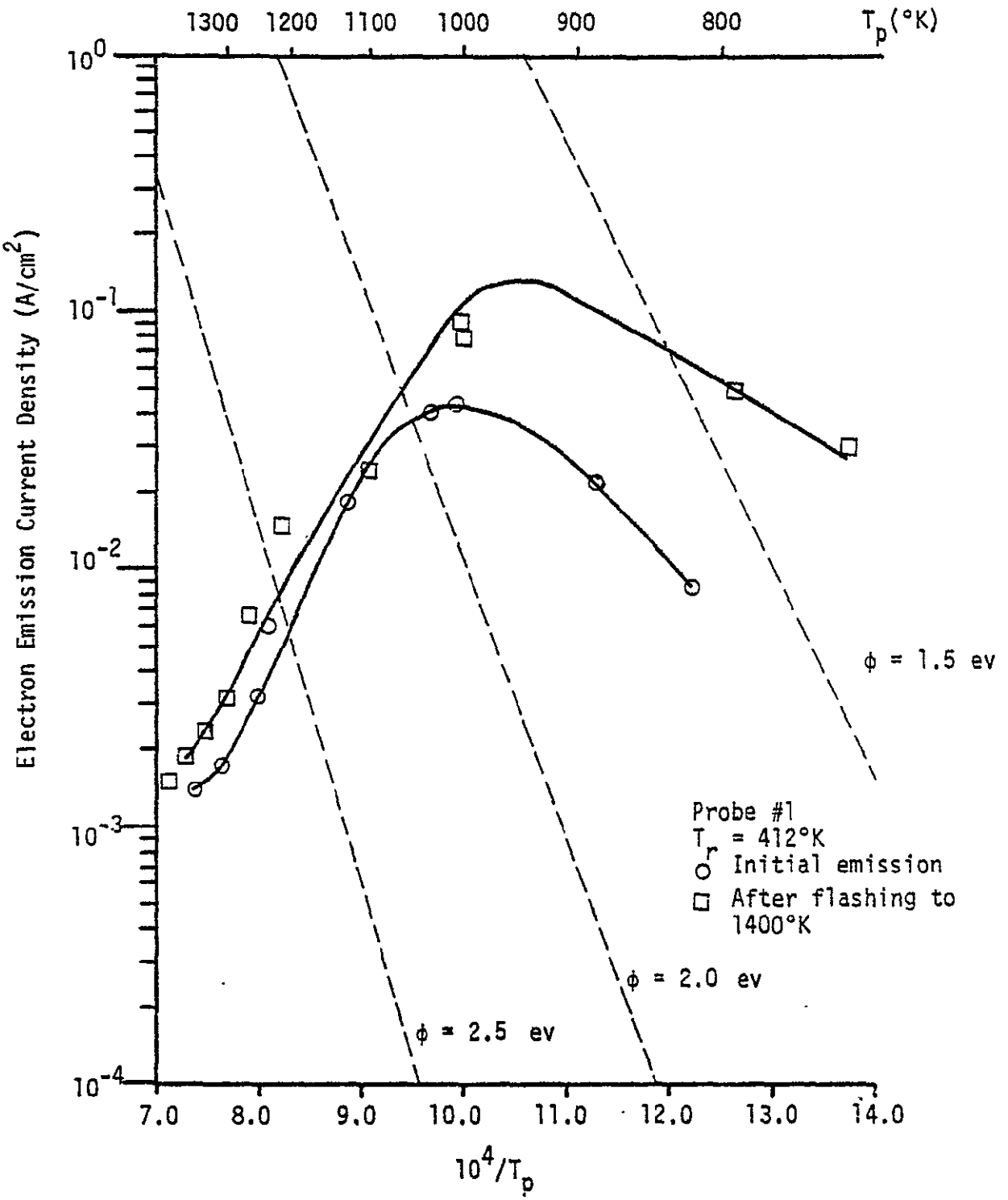

Figure 5. Electron Emission from Nickel

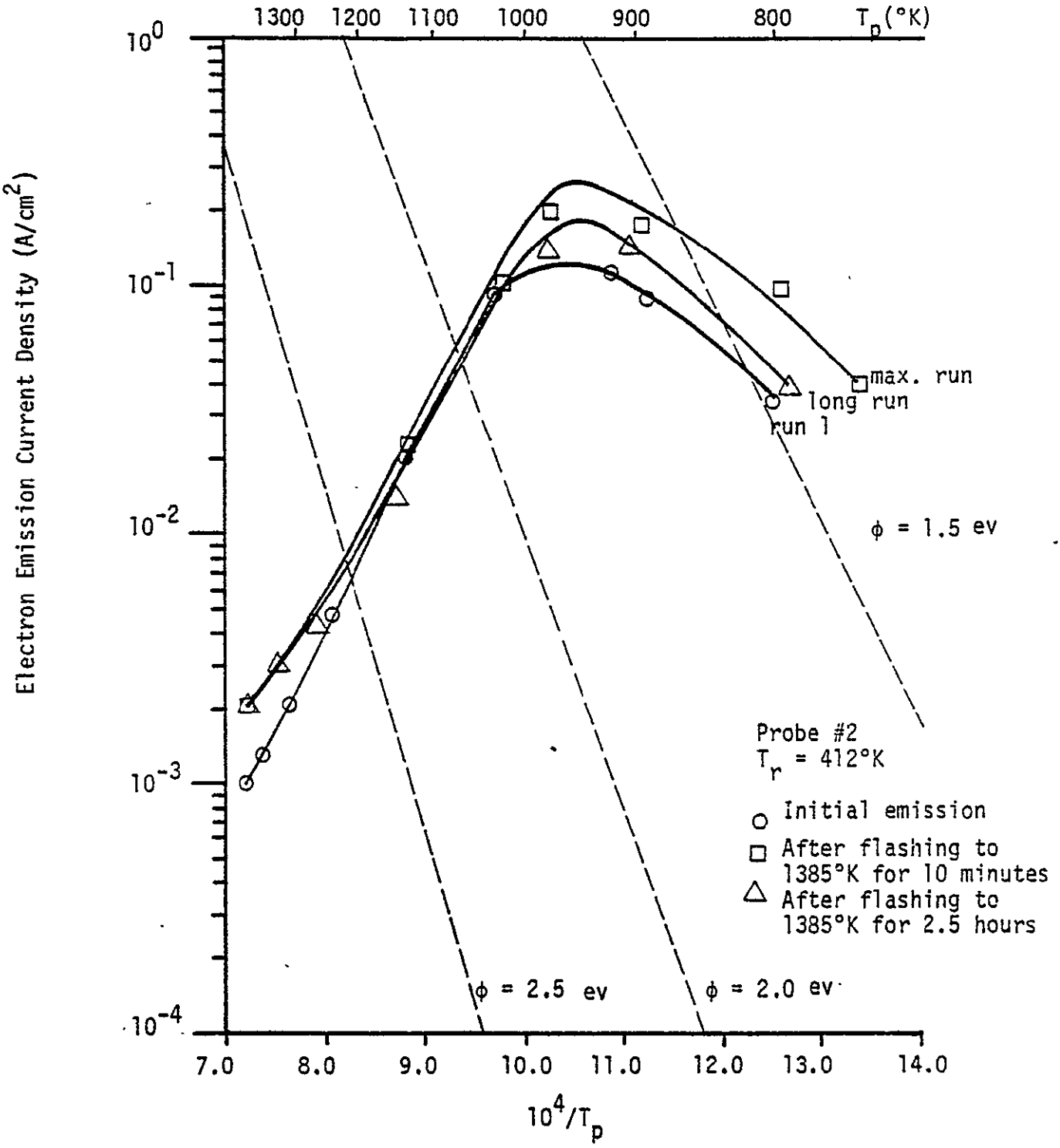

Figure 6. Electron Emission From Inconel† 600

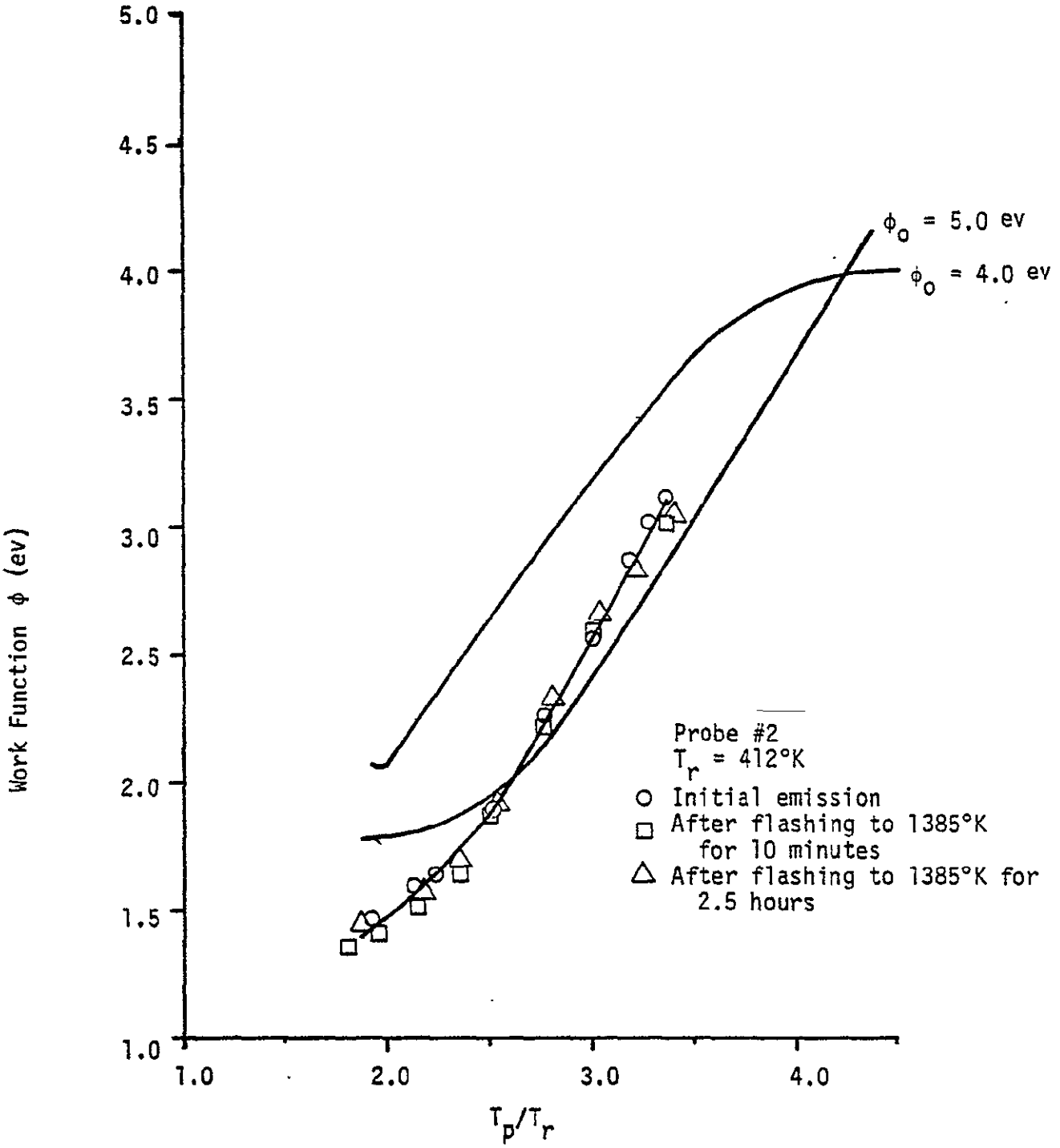

Figure 7. Plot of ϕ vs. T_p/T_r For Inconel† 600

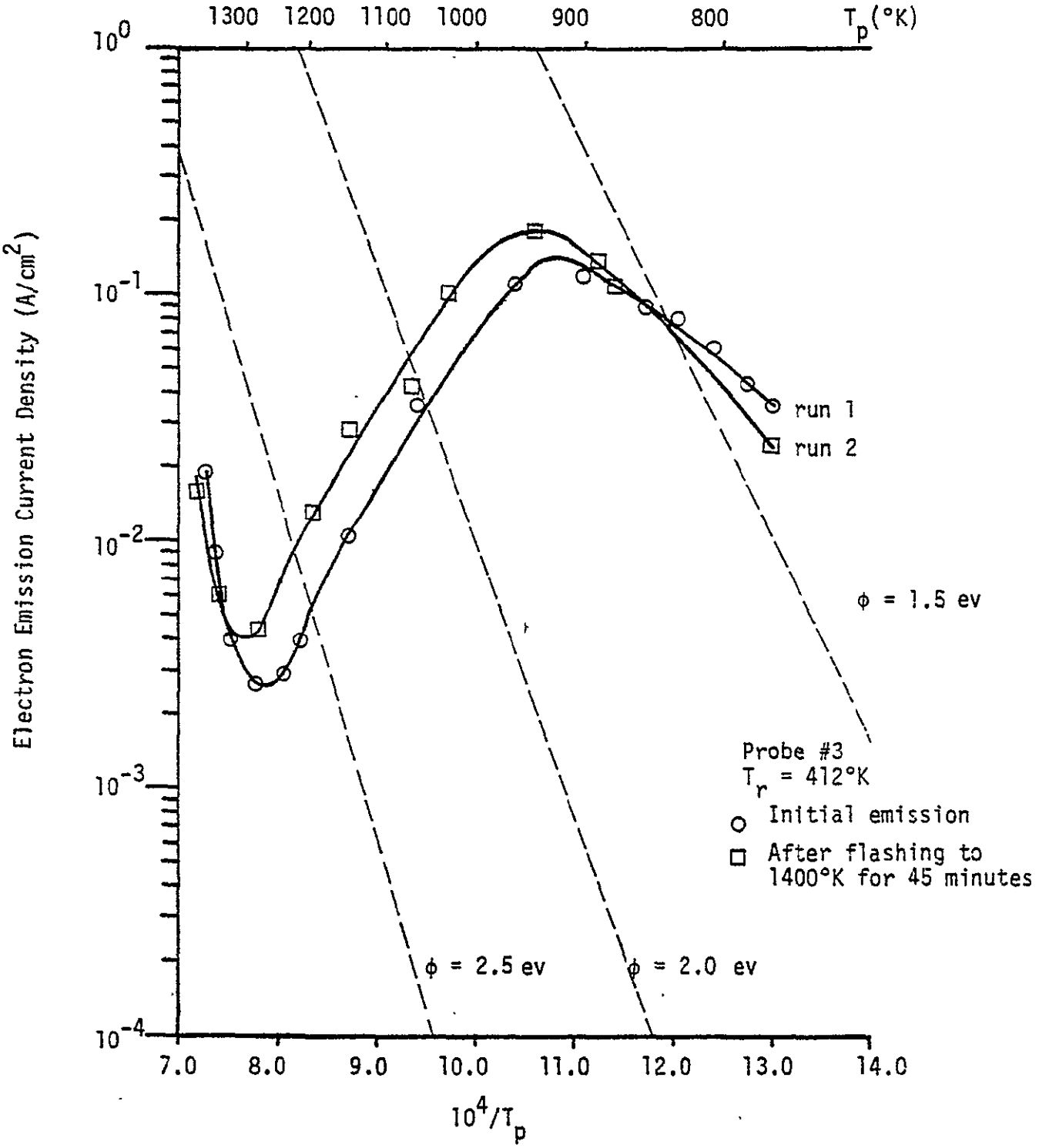

Figure 8. Electron Emission From Hastelloy+ X

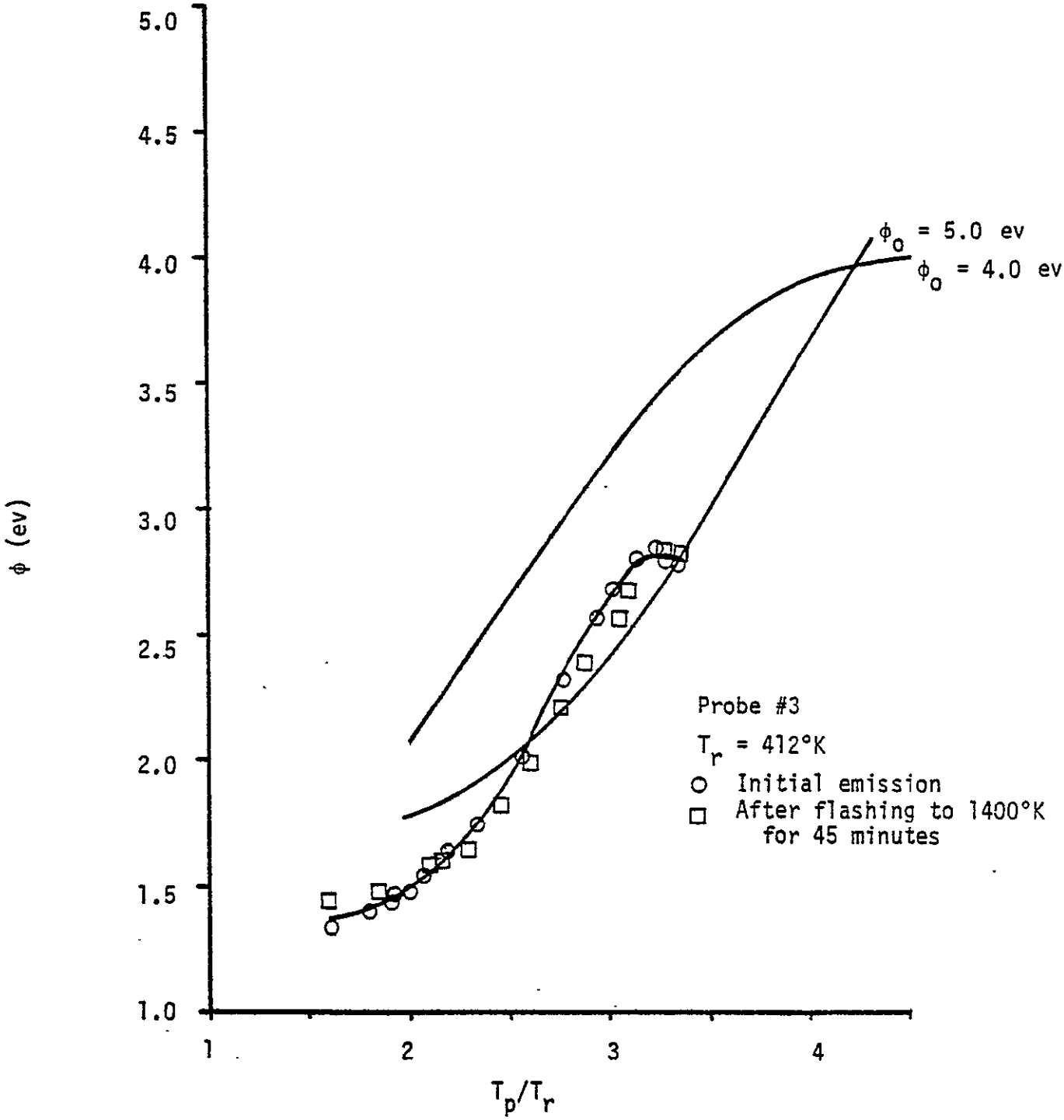

Figure 9. Plot of ϕ vs. T_p/T_r for Hastelloy$^+$ X

REFERENCES

1. P. M. Marchuk, *Trudy Inst. Fiz. Ak. Nauk. Ukraine* **7**, 17 (1956).
2. J. M. Houston and P. K. Dederick, IEEE Proc. Therm. Conv. Spec. Conf., p. 77 (October 1964).
3. J. M. Houston and H. F. Webster, Final Report on Contract AF-19 (628)-4339 (April 1968).
4. J. G. DeSteese, *Appl. Phys. Letters*, **2**, 2 (1963).
5. P. W. Kidd, *J. Appl. Phys.* **36**, 14 (1965).
6. N. S. Rasor and C. Warner, *J. Appl. Phys.* **35**, 2589 (1964).
7. R. G. Wilson, *J. Appl. Phys.*, **37**, 3161 (1966).
8. D. L. Jacobson and E. K. Storms, NASA CR-135063, p. 11 (1976).

REFERENCES

1. Jacobson, D.L. and A.E. Campbell "Molybdenum Work Function Determined by Electron Emission Microscopy." Metallurgical transactions, V. 2 November, 1971, p. 3063-66.

2. Jacobson, D.L. "Fixed Report on Thermionic Converter Research Program" Contract JPL 95 2217, September, 1969.

3. De Steese, J.G. "Electrodes for Thermionic Converters, Phase II-III Final Report" Contract JPL 95 3125, December, 1972.

4. Houston, J.M., Dederick, P.K. "Thermionic Emission of Thermionic Converter Collector Materials in Co Vapor" JEEE Thermionics Conversion Specialist Conference, p. 77-86, 1965.